Article

Adeno-associated virus 2 infection in children with non-A–E hepatitis

https://doi.org/10.1038/s41586-023-05948-2

Received: 21 July 2022

Accepted: 10 March 2023

Published online: 30 March 2023

Check for updates

Antonia Ho[1,206], Richard Orton[1,206], Rachel Tayler[2,206], Patawee Asamaphan[1,206], Vanessa Herder[1,206], Chris Davis[1,206], Lily Tong[1], Katherine Smollett[1], Maria Manali[1], Jay Allan[1], Konrad Rawlik[3], Sarah E. McDonald[1], Elen Vink[1], Louisa Pollock[1,2], Louise Gannon[4], Clair Evans[5], Jim McMenamin[6], Kirsty Roy[6], Kimberly Marsh[6], Titus Divala[6], Matthew T. G. Holden[6], Michael Lockhart[6], David Yirrell[6], Sandra Currie[6], Maureen O'Leary[6], David Henderson[6], Samantha J. Shepherd[7], Celia Jackson[7], Rory Gunson[7], Alasdair MacLean[7], Neil McInnes[7], Amanda Bradley-Stewart[8], Richard Battle[9], Jill A. Hollenbach[10], Paul Henderson[11], Miranda Odam[3], Primrose Chikowore[3], Wilna Oosthuyzen[3], Meera Chand[12], Melissa Shea Hamilton[13], Diego Estrada-Rivadeneyra[13], Michael Levin[13], Nikos Avramidis[3], Erola Pairo-Castineira[3], Veronique Vitart[3,14], Craig Wilkie[15], DIAMONDS Consortium*, ISARIC4C Investigators, Massimo Palmarini[1], Surajit Ray[15], David L. Robertson[1,207], Ana da Silva Filipe[1,207], Brian J. Willett[1,207], Judith Breuer[16,207], Malcolm G. Semple[17,207], David Turner[9,207], J. Kenneth Baillie[3,14,207] & Emma C. Thomson[1,18,207] ✉

An outbreak of acute hepatitis of unknown aetiology in children was reported in Scotland[1] in April 2022 and has now been identified in 35 countries[2]. Several recent studies have suggested an association with human adenovirus with this outbreak, a virus not commonly associated with hepatitis. Here we report a detailed case–control investigation and find an association between adeno-associated virus 2 (AAV2) infection and host genetics in disease susceptibility. Using next-generation sequencing, PCR with reverse transcription, serology and in situ hybridization, we detected recent infection with AAV2 in plasma and liver samples in 26 out of 32 (81%) cases of hepatitis compared with 5 out of 74 (7%) of samples from unaffected individuals. Furthermore, AAV2 was detected within ballooned hepatocytes alongside a prominent T cell infiltrate in liver biopsy samples. In keeping with a $CD4^+$ T-cell-mediated immune pathology, the human leukocyte antigen (HLA) class II *HLA-DRB1*04:01* allele was identified in 25 out of 27 cases (93%) compared with a background frequency of 10 out of 64 (16%; $P = 5.49 \times 10^{-12}$). In summary, we report an outbreak of acute paediatric hepatitis associated with AAV2 infection (most likely acquired as a co-infection with human adenovirus that is usually required as a 'helper virus' to support AAV2 replication) and disease susceptibility related to HLA class II status.

In April 2022, several hospitals in Scotland reported that children were presenting to medical practitioners with acute severe hepatitis of unknown aetiology[1] (Fig. 1a). Elsewhere in the United Kingdom, 270 similar presentations were subsequently reported, for which 15 children required liver transplantation[3]. The World Health Organization (WHO) has now registered 1,010 probable cases that fulfil their definition of this illness in 35 countries[2]. Understanding the underlying cause of this new disease is a global public health imperative.

Detailed clinical investigations carried out as part of the public health response excluded common causes of acute hepatitis, including viral hepatitis, drug toxicity and autoimmune hepatitis. However, recent or active human adenovirus (HAdV) infection was identified in a high proportion of cases in Scotland, England and the United States[4–6]. This finding was notable because HAdV is not a common cause of hepatitis. An increase in HAdV diagnoses in Scotland directly preceded the outbreak of unexplained hepatitis in children of a similar age (Fig. 1a,b).

[1]Medical Research Council–University of Glasgow Centre for Virus Research, Glasgow, UK. [2]Department of Paediatrics, Royal Hospital for Children, Glasgow, UK. [3]Pandemic Science Hub, Centre for Inflammation Research and Roslin Institute, University of Edinburgh, Edinburgh, UK. [4]Department of Paediatrics, NHS Tayside, Dundee, UK. [5]Department of Pathology, Queen Elizabeth University Hospital, Glasgow, UK. [6]Public Health Scotland, Glasgow, UK. [7]West of Scotland Specialist Virology Centre, Glasgow, UK. [8]Virology Laboratory, Ninewells Hospital, Dundee, UK. [9]Histocompatibility and Immunogenetics (H&I) Laboratory, Scottish National Blood Transfusion Service, Edinburgh Royal Infirmary, Edinburgh, UK. [10]Department of Neurology and Department of Epidemiology and Biostatistics, University of California San Francisco, San Francisco, CA, USA. [11]Child Life and Health, University of Edinburgh, Edinburgh, UK. [12]UK Health Security Agency, London, UK. [13]Section of Paediatric Infectious Disease, Department of Infectious Disease, Imperial College London, London, UK. [14]MRC Human Genetics Unit, Institute for Genetics and Cancer, University of Edinburgh, Edinburgh, UK. [15]School of Mathematics and Statistics, University of Glasgow, Glasgow, UK. [16]University College London, London, UK. [17]Pandemic Institute, University of Liverpool, Liverpool, UK. [18]Department of Clinical Research, London School of Hygiene and Tropical Medicine, London, UK. [206]These authors contributed equally: Antonia Ho, Richard Orton, Rachel Tayler, Patawee Asamaphan, Vanessa Herder, Chris Davis. [207]These authors jointly supervised this work: David L. Robertson, Ana da Silva Filipe, Brian J. Willett, Judith Breuer, Malcolm G. Semple, David Turner, J. Kenneth Baillie, Emma C. Thomson. *A list of authors and their affiliations appears online. ✉e-mail: emma.thomson@glasgow.ac.uk

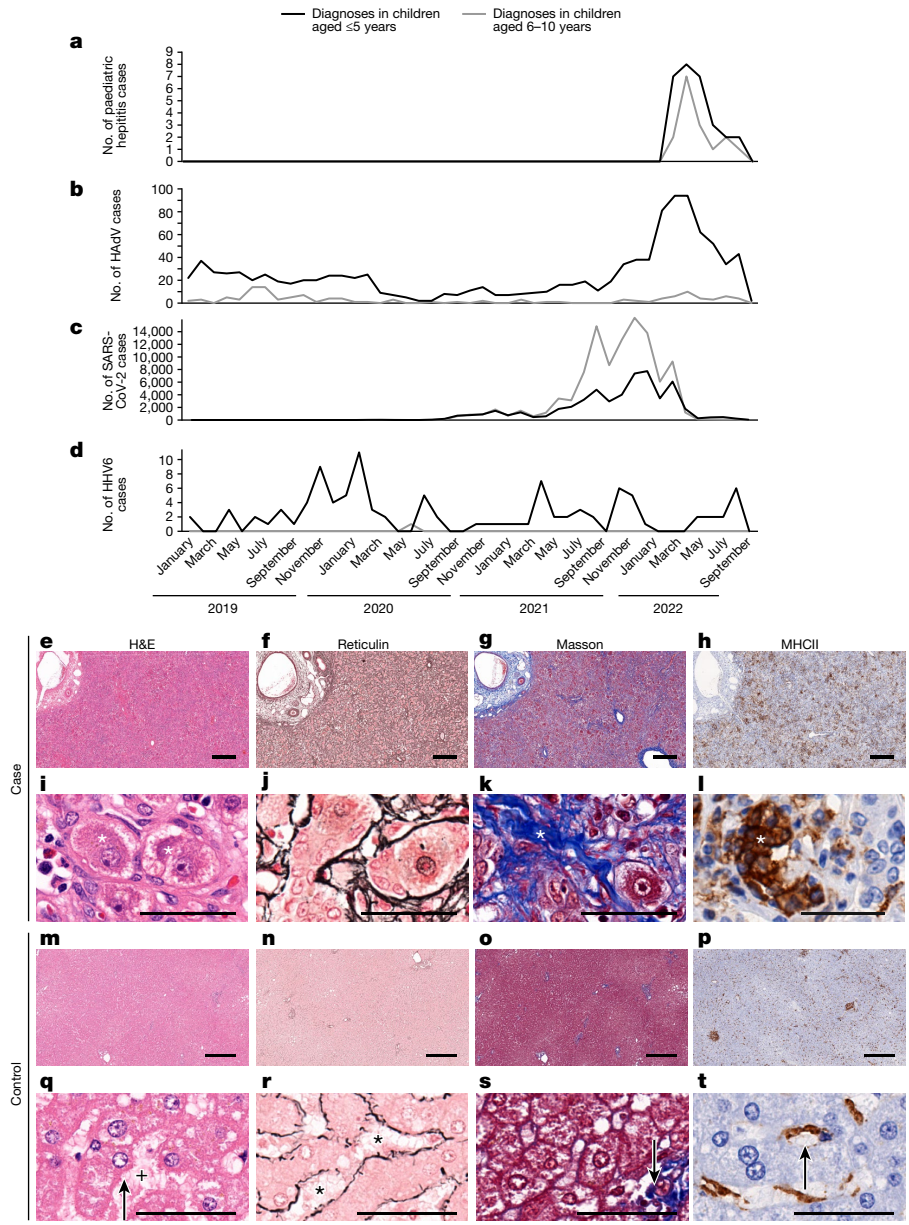

Fig. 1 | Epidemiology and histological appearance of cases of paediatric hepatitis in Scotland. a, The emergence of acute non-A–E hepatitis in children in March–September 2022 (ref. 3). **b**–**d**, Cases of HAdV (**b**), SARS-CoV-2 (**c**) and HHV6 (**d**) infection in children aged ≤10 years in Scotland during the period January 2019 to September 2022. **e**–**t**, Histopathology of samples from cases of non-A–E hepatitis (**e**–**l**) and from healthy liver (**m**–**t**). **e**,**i**,**m**,**q**, Serial sections of formalin-fixed and paraffin-embedded liver tissue sections (one section for each stain per patient sample) stained with haematoxylin and eosin (H&E). **f**,**j**,**n**,**r**, Reticulin staining highlighting structural organization. **g**,**k**,**o**,**s**, Masson staining highlighting collagen fibres. **h**,**l**,**p**,**t**, Staining for MHCII$^+$ cells. **m**–**p**, The regular lobular structure of the liver from a healthy individual (identifier 145783) is not recognisable in **e**–**h**, which are sections collected from patient CVR35 who received a liver transplant. **h**, Immunohistochemistry showed an increase in MHCII$^+$ cells in tissue samples from patient CVR35 compared with healthy liver (**l**,**t**). **i**–**l**, Higher magnification micrographs of **e**–**h** showing details of liver histopathology. **i**,**q**, For patient CVR35 (**i**), enlarged (ballooned) and vacuolated hepatocytes (marked by asterisks) are evident compared with hepatocytes in healthy liver (**q**; from individual 145783) with regular morphology (indicated by the arrow) and regular sinus (indicated by the plus symbol). **j**,**r**, For the sample from patient CVR35 (**j**), reticulin staining shows destruction of the sinus structures and irregularly arranged fibres, whereas healthy liver (**r**) shows fibres lining the sinus (indicated by asterisks). **k**,**s**, For the sample from patient CVR35 (**k**), Masson staining shows an increase in collagen fibres (in blue, indicated by the asterisk) compared with minimal staining of fibres (indicated by the arrow) in healthy liver (**s**). **l**,**t**, High magnification image showing accumulation of MHCII$^+$ cells in the liver (indicated by the asterisk) of patient CVR35 (**l**), whereas healthy liver (**t**), staining is limited to Kupffer cells (indicated by the arrow). Scale bars, 50 µm (**i**–**l**,**q**–**t**) or 400 µm (**e**–**h**,**m**–**p**).

SARS-CoV-2 had been circulating for 2 years and peaked several months before the increase in hepatitis cases[3] (Fig. 1c). Human herpesvirus 6 (HHV6A and HHV6B) infections were not detected at higher levels during 2021 or 2022 (Fig. 1d).

Research investigation

To investigate the aetiology of these cases of acute hepatitis, we recruited 32 affected children who presented to a hospital between 14 March 2022

and 20 August 2022 and met the Public Health Scotland case definition criteria for inclusion in the International Severe Acute Respiratory and Emerging Infections Consortium (ISARIC) WHO Clinical Characterization Protocol United Kingdom (CCP-UK) (ISRCTN66726260)[7]. Samples from unaffected children (control samples) were obtained from the Diagnosis and Management of Febrile Illness using RNA Personalised Molecular Signature Diagnosis (DIAMONDS) study cohort and from the NHS Greater Glasgow & Clyde (GG&C) Biorepository under appropriate ethics approval (Methods)

Clinical presentation

The median age of affected patients was 4.1 years (interquartile range (IQR) of 2.7–5.5 years) (Table 1). All patients were of white ethnicity, and 21 out of 32 (66%) were girls. Eighteen (56%) of the children reported a subacute history 2–12 weeks before acute hepatitis, which was characterized by an initial gastroenteritis-like illness followed by intermittent vomiting, abdominal pain and fatigue. The majority (23 out of 32) had no other medical conditions. One child had previously received a liver transplant, whereas none of the other patients were immunocompromised and none had received a COVID-19 vaccination. All routine blood tests for viral hepatitis, including hepatitis A, B, C and E, acute Epstein–Barr virus (EBV), cytomegalovirus (CMV), HHV6 and HHV7, and herpes simplex virus (HSV) were negative (Supplementary Table 1). Four patients had a low titre (1:80) of anti-nuclear antibodies and 3 patients had a low titre (1:40) of anti-smooth muscle antibodies, but other markers of autoimmunity were negative (Table 1 and Supplementary Table 2).

Following hospitalization, liver biopsy samples were obtained from five children. The samples showed evidence of lobular hepatitis with periportal and interface inflammation, intracellular inclusions, bile duct proliferation and ballooning of hepatocytes of varying severity (Fig. 1e–t). Mild-to-moderate fibrotic changes were noted, with no evidence of confluent fibrosis, and there was an inflammatory infiltrate that included cells expressing major histocompatibility complex class II (MHCII). Modified hepatic activity index scores (Ishak system)[8,9] ranged from 6 to 11 (Extended Data Table 1), and the biopsy samples stained negative for complement.

Four patients required transfer to a specialist liver unit owing to significant synthetic liver dysfunction. Two of the patients were treated with steroid therapy and improved. One patient received supportive care only and spontaneously improved. The fourth patient had severe disease and required liver transplantation and was treated with cidofovir for HAdV viraemia and steroids after the liver transplant. The remaining 28 patients received supportive care only, with no antiviral or steroid treatment, and all showed gradual resolution of hepatitis over 2–3 months. There were no deaths. The median duration of hospital stay was 6 days (range of 1–68 days) (Table 1). In the patients with weakly positive autoantibodies, all had normal or normalizing transaminase levels at last follow up in the absence of treatment with an anti-inflammatory or immunosuppressant.

Table 1 | Demographic and clinical characteristics of the 32 patients with unexplained hepatitis

Demographics	Results
Age (years)[a]	4.1 (2.7–5.5, 0.9–10.6)
Sex (girls)[b]	20 (63%)
Co-morbidity[b]	9 (28%)[c]
Biochemistry	
Peak bilirubin[a] (μmol l^{-1})	82 (36–160, 3–387)
Peak alanine transaminase[a] (U l^{-1})	1,757 (708–2,763, 333–5,417)
Peak aspartate transaminase[a] (U l^{-1})	2,048 (833–3,408, 424–6,908)
Peak γ-glutamyltransferase[a] (U l^{-1})	124 (91–162, 18–720)
Peak international normalized ratio[a]	1.2 (1.1–1.4, 1.0–2.9)
Peak C-reactive protein[a] (mg l^{-1})	5 (3–11, 1–117)
Caeruloplasmin[a] (n=24) (g l^{-1})	0.36 (0.33–0.39, 0.22–0.52)
Key autoimmune parameters	
IgG[a] (g l^{-1})	11.8 (9.9–14.3, 1.5–21.0)
Coeliac screen (TTG antibody) (n=26)	26 normal range
Anti-mitochondrial antibody	32 negative
Anti-smooth muscle antibody	29 negative, 3 low positive (1:40)[c]
Anti-liver kidney microsomal 1 antibody	32 negative
Anti-nuclear antibody	28 negative, 4 weak positive 1:80 titre[c]
Clinical presentation	
Symptoms at presentation[b]	
• Vomiting	22 (69%)
• Jaundice	21 (66%)
• Poor appetite	12 (38%)
• Lethargy or fatigue	10 (31%)
• Abdominal pain	10 (31%)
• Diarrhoea	4 (13%)
Subacute symptoms for ≥14 days before presentation (n=32)	18 (56%)
Subacute symptoms reported (n=18)	
• Intermittent vomiting	15 (83%)
• Initial gastroenteritis-like illness	12 (67%)
• Abdominal pain	9 (50%)
• Lethargy or fatigue	7 (39%)
• Poor appetite	6 (33%)
• Weight loss	6 (33%)
Approximate duration of subacute symptoms before presentation[a,d]	42 (27–52, 14–85) days
Length of hospital stay[a,e]	6 (4–10, 1–68) days
Required transfer to tertiary liver unit	4 (12.5%)
Required liver transplant	1 (3%)

[a]Median (IQR, range). [b]Number (%) denominator=32 unless otherwise specified. [c]See Supplementary Information for additional clinical details. [d]n=16 patients with data available. [e]n=30, one patient was a long-term in-patient for an unrelated condition, one patient was managed as an outpatient.

Pathogen detection by sequencing

As the epidemiology was in keeping with the emergence of an infectious pathogen, we undertook metagenomics and target enrichment (TE) next-generation sequencing (NGS) on all available clinical samples from the first nine recruited patients. The samples included plasma (n = 9), liver biopsy samples (n = 4), throat swabs (n = 6), faecal samples (n = 7) and a rectal swab (n = 1), and an average of 14 million sequence reads per sample were obtained (Fig. 2a–d). The samples were obtained between 7 and 80 days after initial symptom onset. Samples from the control group were restricted to children recruited in the United Kingdom between January 2020 and April 2022. Two comparison groups were used as controls: group 1 comprised serum or plasma samples from 13 age-matched healthy children (10 boys, 3 girls; age range of 3–5 years); and group 2 comprised serum or plasma samples from 12 children (8 boys, 4 girls; age range of 1–4 years) with HAdV infection confirmed by PCR and with normal transaminase levels. The children in group 2 had been diagnosed by nasopharyngeal aspirate (n = 10), by nose swab (n = 1) or by stool (n = 1) as part of the routine clinical investigation process and half of the patients required critical

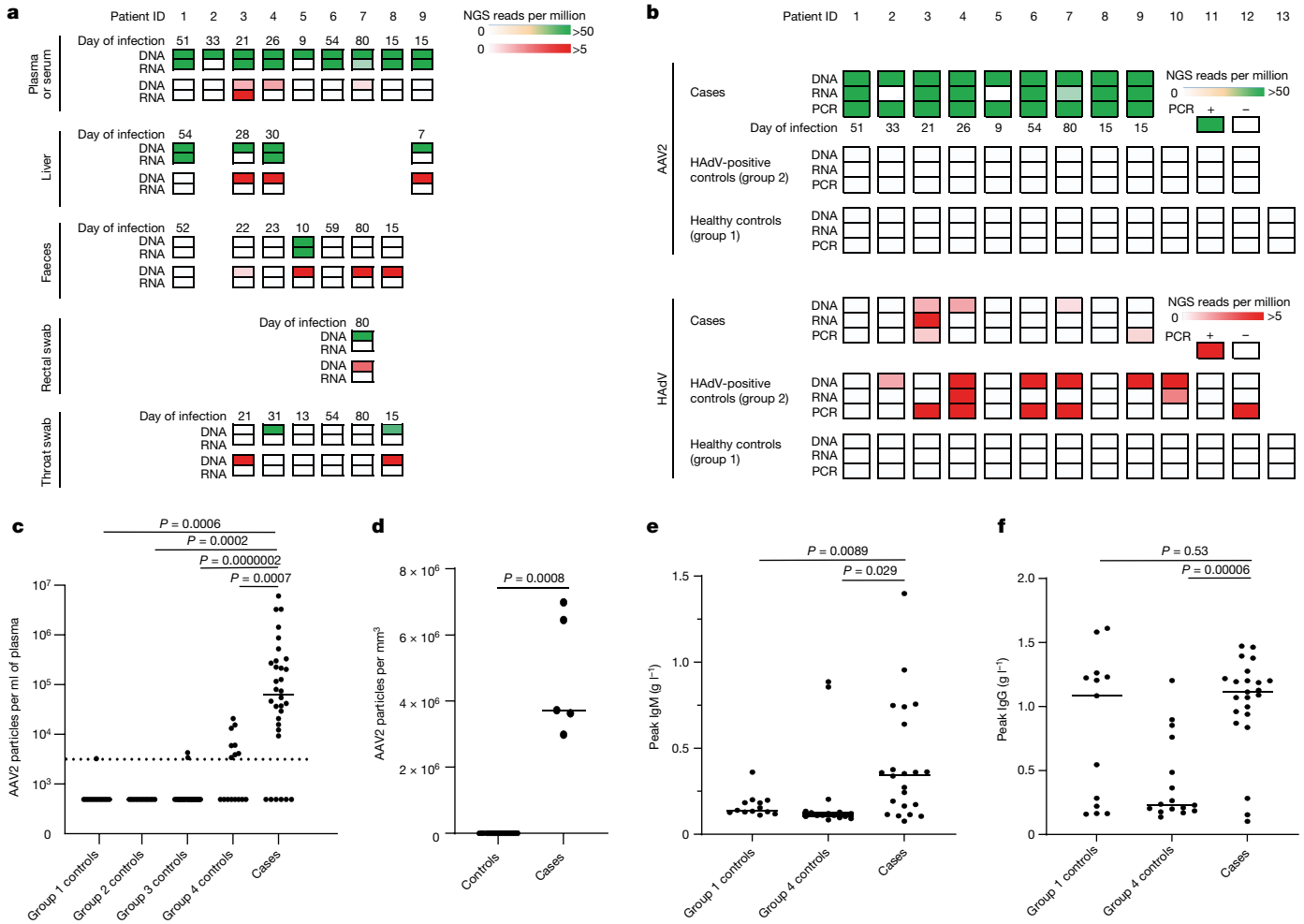

Fig. 2 | Detection of AAV2 in cases of paediatric hepatitis. a, Heatmap of HAdV and AAV2 reads detected in cases of hepatitis by TE sequencing. Samples obtained for routine clinical investigation (plasma, liver, faeces, rectal swab and throat swab) were retrospectively sequenced following DNA or RNA extraction. AAV2 read counts are shown from 0 to >50 reads per million in green (top rows) and HAdV read counts are shown from 0 to >5 reads per million in red (bottom rows). **b**, Heatmap of viral reads of plasma samples from cases of hepatitis and of plasma or sera samples from controls. Plasma samples from cases of hepatitis (cases), and plasma or sera samples from children with HAdV infection (group 2 controls) and from age-matched healthy children (group 1 controls) were sequenced following DNA or RNA extraction. AAV2 read counts are shown from 0 to >50 reads per million in green and HAdV read counts are shown from 0 to >5 reads per million in red. The number of days between initial symptom onset and sample are indicated. **c**, AAV2 real-time RT–qPCR of serum or plasma samples from 32 cases of hepatitis (cases) and from 74 controls in four groups: 13 in group 1 (healthy controls); 12 in group 2 (HAdV-positive controls); 33 in group 3 (hepatitis controls); and 16 in group 4 (contemporaneous controls). The detection threshold of the assay (3,200 copies per ml) is shown as a dotted line. Values are shown as a scatter plot with a median line. **d**, AAV2 real-time RT–qPCR of liver biopsy samples from 5 cases of hepatitis and from 19 controls. **e**, IgM responses determined by ELISA in 22 cases of hepatitis and in 29 controls (13 in group 3, 16 in group 4). **f**, IgG responses determined by ELISA in 22 cases of hepatitis cases and in 29 controls (13 in group 3, 16 in group 4). For **c**–**f**, statistical analysis was performed using Mann Whitney test (two-tailed), and experiments were performed in triplicate.

care. The difference in age between the patients with hepatitis and the healthy children in group 1 was not significant, but some samples from group 1 were obtained earlier than samples from the cases of hepatitis (January 2020–April 2022 compared with March–April 2022, respectively) (Extended Data Table 2a). The children in group 2 were younger (median age of 1.4 years, IQR of 1.1–3.1 years, $P < 0.001$), and samples were obtained between May 2020 and December 2021 (Extended Data Table 2b). Metagenomics NGS was carried out using protocols designed to identify both RNA and DNA viruses. Semi-agnostic TE sequencing was also performed using VirCapSeq-VERT Capture probes that target the genomes of 207 taxa of viruses known to infect vertebrates.

TE sequencing reflected the metagenomics NGS results, but with higher sensitivity, and correlated with viral loads measured by quantitative PCR with reverse transcription (RT–qPCR) (Supplementary Figs. 1 and 2). The results from both methods showed that the viral genome detected most frequently in affected patient plasma samples was AAV2 (9 out of 9 cases) (Fig. 2a, Supplementary Table 3 and Extended Data Fig. 1). AAV2 was also detected in 4 out of 4 liver biopsy samples, and in 1 out of 7 faecal samples, 1 out of 1 rectal sample and 1 out of 6 throat swab samples. At lower read counts, HAdV-F41 or HAdV-C was detected in 6 out of 9 patients, whereas HHV6B was detected in 3 out of 4 plasma samples (Extended Data Fig. 1, Supplementary Tables 4 and 5, Supplementary Data 1 and Supplementary Fig. 3). HAdV types C1, 2, 5 and 6 could not be reliably distinguished owing to low read counts. The remaining clinical samples were excluded from analysis for HHV by sequencing because murine herpesvirus 1 had been added as an extraction control during routine clinical investigation.

Read counts of AAV2 by TE sequencing were high (median of 4,478 reads per million, IQR of 774–10,498 reads per million) in all 9 out of 9 cases of hepatitis compared with 0 out of 13 in group 1 healthy controls (IQR of 0–0 reads per million, $P < 0.001$) and 0 out of 12 in group 2 controls (children with HAdV infection and normal liver function tests;

IQR of 0–0 reads per million, $P < 0.001$) (Supplementary Table 5). HAdV reads were detected in 6 out of 12 HAdV-positive samples from group 2 controls (median of 0.82 reads per million, IQR of 0–1,053 reads per million) despite plasma or sera being a suboptimal sample type to detect HAdV. HAdV was detected in 3 out of 9 cases of hepatitis (median of 0 reads per million, IQR of 0–0.6 reads per million), whereas 0 out of 13 was detected in group 1 healthy controls (IQR of 0–0 reads per million, $P = 0.055$). HHV6B was also detected in 3 out of 4 cases of hepatitis compared with 0 out of 13 healthy controls (median of 1.9 reads per million, IQR of 0.3–3.5 reads per million and IQR of 0–0 reads per million, respectively, $P = 0.006$) (Supplementary Table 4). However, HHV6B read counts did not differ significantly between cases of hepatitis and group 2 controls (median of 0 reads per million, IQR of 0–0.04 reads per million, $P = 0.16$), which is in keeping with the occurrence of reactivation of HHV6B in the context of severe illness. The metagenomics and TE sequencing results from the 13 age-matched healthy control samples (group 1) revealed no evidence of AAV2, HAdV or HHV6B in plasma; however, low read counts of EBV, CMV and HHV6A were detected in a small number of samples (Supplementary Table 4). In samples from group 2 (children with HAdV infection and normal liver function tests), herpesviruses were detected in 9 out of 12 samples, including 2 out of 12 (as described above) with detectable numbers of HHV6B reads (1,050 and 5,062 reads per million), which was confirmed by PCR.

Sequence and phylogenetic analyses

Near-full genomes of AAV2 were obtained from all nine patients with hepatitis (GenBank accession numbers OP019741–OP019749), and in all cases, two large open reading frames corresponding to the *rep* and *cap* genes, flanked by inverted terminal repeat regions, were identified. Seven distinct sequences of AAV2 were noted (Extended Data Fig. 2), forming a single clade, alongside four AAV2 genomes previously detected in France between 2004 and 2015. Two out of three identical sequences were known to have come from individuals from the same household, therefore these two are epidemiologically linked. The third sequence was from a sample obtained around the same time but was not known to be linked to the other cases. Sequences from the liver samples matched those detected in plasma. Several mutations within the *VP1–VP3* genes were noted to be over-represented in the sequences derived from patients with hepatitis when compared with reference sequences (Extended Data Fig. 2). Notably, nine of the mutations in the capsid gene that were over-represented in the cases of hepatitis (V151A, R447K, T450A, Q457M, S492A, E499D, F533Y, R585S and R588T) are associated with an AAV2 variant that has an altered phenotype. Characteristics of this variant include substantial evasion of neutralizing antibodies directed against wild-type AAV2, enhanced production yields, reduced heparin binding, increased virion stability and more localized spread in a mouse model[10].

A full genome of HAdV-F41 was obtained from a faecal sample (GenBank accession number OP019750) and was found to be closest phylogenetically to two genomes reported from Germany in 2019 and 2022 (Extended Data Fig. 2). Contigs matching to other human pathogens, including human coronavirus NL63, rhinovirus C, enterovirus B, human parainfluenza viruses 2 and 3, norovirus, and both betaherpesvirus and gammaherpesvirus were also detected across cases, albeit not consistently. These findings were confirmed by PCR (Supplementary Table 1).

Confirmatory PCR testing of cases of hepatitis

PCR testing for AAV2 was positive in all nine initial cases of hepatitis. Standards were used to estimate the viral loads of positive samples (Supplementary Fig. 2). All nine plasma samples tested negative by PCR for HHV6, HSV, CMV and EBV. Two out of the four liver biopsy specimens tested positive for HHV6 (cycle threshold (Ct) values of 33 and 36) (Supplementary Table 1). HAdV was detected in 3 out of 9 plasma samples, 3 out of 4 liver biopsy samples, 2 out of 6 throat swabs, 4 out of 7 faecal samples and 1 out of 1 rectal swab. The lower detection of HAdV and HHV6 by PCR compared with TE sequencing probably reflects a slightly lower sensitivity of the PCR assay. The low numbers of HAdV-positive samples detected using both assays may reflect the fact that plasma is a suboptimal sample type for HAdV detection (whole blood samples were unavailable).

Case–control study

To investigate the presence of AAV2 and the candidate helper viruses HAdV and HHV6B in plasma samples from cases of hepatitis, we undertook a case–control study in which samples from 32 cases of hepatitis were compared with samples from the group 1 and group 2 controls described above and with samples from two additional control groups (Fig. 2a–f). Group 3 controls comprised 33 children (18 boys and 15 girls aged 2–16 years) with increased transaminase levels that had tested negative by PCR for HAdV. This group was used to test the hypothesis that reactivation of AAV2 may occur in children with severe hepatitis and may be a correlate of liver dysfunction. The children comprising group 3 were older (median age of 10.2 years, IQR of 7–13.6 years, $P < 0.001$) than the patients from the case group (Extended Data Table 2b) and 15 out of 33 had required critical care for ventilatory or cardiovascular support. Group 4 controls comprised residual plasma or serum samples from 16 children in Scotland aged 10 years and were attending hospital contemporaneously with the children with hepatitis between March and April 2022. The group 4 controls were used to determine whether AAV2 was circulating widely in children in healthcare facilities across Scotland at the time the children with hepatitis were admitted to hospital. Clinical details, including liver function were not available for this group. To ensure that the quantification of AAV2 was accurately performed, we confirmed standard curve concentrations using droplet digital PCR (Methods).

Significance differences between groups for viral loads in plasma samples were calculated using a Mann–Whitney test (two-tailed). RT–qPCR of plasma samples showed that 26 out of 32 cases of hepatitis were positive for AAV2, with a median estimated copy number of 66,100 copies per ml (IQR of 13,461– 300,277 copies per ml), a value higher than samples from all the control groups ($P < 0.001$ for all case–control comparisons). The median copy number in control groups 1–3 was below the detection limit. A median of 3,268 copies per ml (detection threshold of 3,200 copies per ml) was present in samples from control group 4, which suggested that AAV2 was circulating at low levels in children during March and April 2022 (Fig. 2c). Although five plasma samples from cases of hepatitis were positive for HAdV by PCR, and one tested positive by PCR for HHV6 DNA, these results were not significantly more common than in samples from the control group (Supplementary Fig. 3).

Next, five liver biopsy samples from cases of hepatitis were compared with 19 residual liver biopsy samples (controls) from children under 18 years old. The median AAV2 viral load was 3,721,497 copies per mm^3 of liver (IQR of 3,308,243–6,717,616 copies per mm^3) in cases of hepatitis compared with 64 copies per mm^3 of liver (IQR of 20–83 copies per mm^3) in samples from the control group ($P < 0.001$; Fig. 2d). Glyceraldehyde-3-phosphate dehydrogenase was used as a marker of extraction efficiency in all samples, and results were similar between the case and control groups. When outliers were removed, significance was retained (Supplementary Data 2, Supplementary Fig. 4).

Longitudinal sampling

To investigate AAV2 viraemia and liver function values over time, longitudinal PCR testing was performed in 14 cases of hepatitis from whom multiple retrospective plasma samples were available (Supplementary Fig. 5). Spearman's rank correlation coefficients for the relationships

between the trajectories of viral load and alanine transaminase and bilirubin were positive for most cases. However, overall statistical significance could not be confirmed owing to the sample size.

Where samples were available, we screened for the presence of AAV2-specific IgM and IgG antibodies within samples from patients and samples from the group 1 healthy controls and group 4 contemporaneous controls (Fig. 2e,f and Supplementary Fig. 6). Anti-AAV2 IgM was detected in 15 out of 23 (65.2%) samples from cases of hepatitis, but only 1 out of 13 (7.7%) samples from group 1 healthy controls and 2 out of 16 (12.5%) samples from the group 4 contemporaneous controls from Scotland. For the samples from cases of hepatitis that tested negative for AAV2-specific IgM, samples from four patients were noted to be obtained fewer than 3 days after the onset of illness and samples from two patients were obtained more than 77 days after the onset of illness. IgG was detected in 21 out of 23 (91.3%) samples from cases of hepatitis, in 8 out of 13 (61.5%) samples from age-matched healthy controls (group 1) and in 9 out of 16 (56.3%) samples from healthy controls from Scotland (group 4). Of the two samples from patients who tested seronegative, both were obtained at early time points, probably sampled before expected seroconversion (less than 3 days after the onset of illness).

SARS-CoV-2 infection

Routine clinical investigation detected SARS-CoV-2 nucleic acid in nasopharyngeal samples from 3 out of 31 (9.6%) children at the time of illness, 2 of whom were also seropositive. The third became infected after the onset of hepatitis. SARS-CoV-2 was not detected by PCR or by sequencing in any of the samples from cases or controls available for analysis, including liver samples. Nevertheless, to investigate the possibility that unexplained hepatitis in children might relate to a previous infection with SARS-CoV-2 or other seasonal coronaviruses, we carried out serological analysis of 23 available residual samples from cases. IgG antibody titres were quantitatively measured against the spike protein, the amino-terminal domain (NTD) and receptor binding domain (RBD) of the spike protein and the nucleocapsid of SARS-CoV-2. IgG antibody titres were also measured for human seasonal coronaviruses 229E, OC43, NL63 and HKU1. Electrochemiluminescence assays (MSD-ECL) for coronavirus-specific IgG revealed previous exposure to seasonal coronaviruses, with strong responses detected against NL63 (17 out of 23) and OC43 (21 out of 23) (Extended Data Fig. 3a). By comparison, plasma samples from 12 out of 23 children displayed high reactivity against HKU1, whereas only 3 out of 23 samples reacted strongly against 229E. Plasma samples from 11 children reacted with 2 or more SARS-CoV-2 antigens (nucleocapsid, spike protein, NTD or RBD). One of the samples reacted solely with the nucleocapsid antigen, which indicated that in total, 12 out of 23 patients displayed serological evidence of previous exposure to SARS-CoV-2 (Extended Data Fig. 3b). In summary, 12 out of 23 (52%) of the children with hepatitis displayed evidence of previous exposure to SARS-CoV-2. This level is lower than SARS-CoV-2 seroprevalence in children aged 5–11 years in Scotland between 14 March and 27 June 2022 (when Public Health Scotland enhanced surveillance for COVID-19 was discontinued), which was reported as between 59.0% (95% confidence interval (CI) of 50.6–71.2) and 72.4% (95% CI of 53.9–78.8)[11]. This result indicates that there is no direct link between COVID-19 and the outbreak of acute hepatitis studied here.

Host genetics and HLA typing

We next investigated whether some children might be genetically more susceptible to non-A–E hepatitis. To that end, 27 samples from cases of hepatitis and 64 platelet apheresis samples from local donors in Scotland (controls) were genotyped using high-resolution typing for all HLA loci (*HLA-A*, *HLA-B*, *HLA-C*, *HLA-DRB1*, *HLA-DRB3*, *HLA-DRB4*, *HLA-DRB5*, *HLA-DQA1*, *HLA-DQB1*, *HLA-DPA1* and *HLA-DPB1*). In total, 25 out of 27 (92.6%) samples from patients with hepatitis were positive for at least one copy of the *HLA-DRB1*04:01* allele compared with 10 out of 64 (15.6%) of samples from controls. The allele frequency in patients was 0.54 compared with 0.08 in controls (odds ratio (OR) of 13.7 (95% CI of 5.5–35.1), $P = 5.49 \times 10^{-12}$). The frequency of the *HLA-DRB1*04:01* allele (based on an imputation of HLA alleles) in a control set of unrelated participants from the UK Biobank ($n = 29{,}379$) was 0.11 (2,942 out of 29,379 allele carriers, OR of 112.3 (95% CI of 26.6–474.5), $P = 3.27 \times 10^{-23}$). The frequency was also 0.11 in British/Irish North-West European individuals from the Anthony Nolan charity register[11]. To check for cryptic relatedness among patients and population stratification, we performed genome-wide microarray genotyping in 19 cases of hepatitis and excluded participants with a conservative relatedness threshold (identity-by-state > 0.4). When compared with well-matched participants from the UK Biobank (Extended Data Fig. 4), similar signals for association with disease by allele frequency ($P = 8.96 \times 10^{-6}$) and across the three possible biallelic genotypes at this locus ($P = 1.2 \times 10^{-9}$) were obtained.

In addition to the association with the *DRB1* allele, 23 out of 27 samples from patients with hepatitis were positive for *HLA-DQA1*03:03* compared with 11 out of 64 samples from controls (allele frequency of 0.54 compared with 0.09, respectively, OR of 12.3 (5.1–30.7), $P = 1.9 \times 10^{-11}$). Moreover, 26 out of 27 samples from patients were positive for *HLA-DRB4*01:03* compared with 21 out of 64 samples from controls (allele frequency of 0.67 compared with 0.17, respectively, OR of 9.4 (4.4–21.3), $P = 1.8 \times 10^{-10}$). Owing to strong linkage disequilibrium in this region of the genome, it is not possible to be certain which is the causal susceptibility allele.

In situ hybridization and immune typing

To investigate the presence of AAV2, HAdV and HHV6 in liver biopsy samples, we carried out in situ hybridization (ISH). Liver biopsy samples of all patients were characterized by the presence of AAV2 RNA within the nuclei and cytoplasm of ballooned hepatocytes and in arterial endothelial cells, which is indicative of the presence of replicating virus (Fig. 3a–h). AAV2-positive cells were quantified at a high level in all cases using QuPath in biopsy samples from five non-A-non-E hepatitis, ranging from 1.2 to 4.7%. This level is similar to that seen in hepatitis associated with other viruses[12,13]. Consistent with low levels of HHV6B and HAdV sequence reads present in the biopsy samples from cases of hepatitis, negligible levels of viral RNA from these viruses were detected by ISH.

To investigate the possibility of an immune-mediated pathogenesis of disease in the liver, multiplex analysis of liver samples was carried out using co-detection by indexing (CODEX) for various immune cellular markers, including CD3, CD4, CD8, PD-L1, CD107a, CD20, CD31, CD44, CD68, MX1 and PanCK (Fig. 4a–d and Supplementary Figs. 7 and 8). In the explant liver sample of patient CVR35, prominent disordered proliferation of epithelial cells throughout the liver tissue was evident, with increased numbers of $CD68^+$ macrophages, activated $CD4^+$ and $CD8^+$ T cells and $CD20^+$ B cells. High expression of the interferon-induced GTP-binding protein MX1 was also noted, which indicated that the innate immune response was activated.

Conclusions and final statements

In this study, we reported the association of AAV2 infection and the class II HLA allele *HLA-DRB1*04:01* with an outbreak of paediatric non-A–E hepatitis, with virus being detected independently by sequencing, real-time PCR and ISH. Liver biopsy tissue samples from all patients were characterized by the presence of AAV2 RNA (indicating replicating virus) within the nucleus and cytoplasm of ballooned hepatocytes and by a dense infiltrate of $CD4^+$ and $CD8^+$ T cells in the liver with an

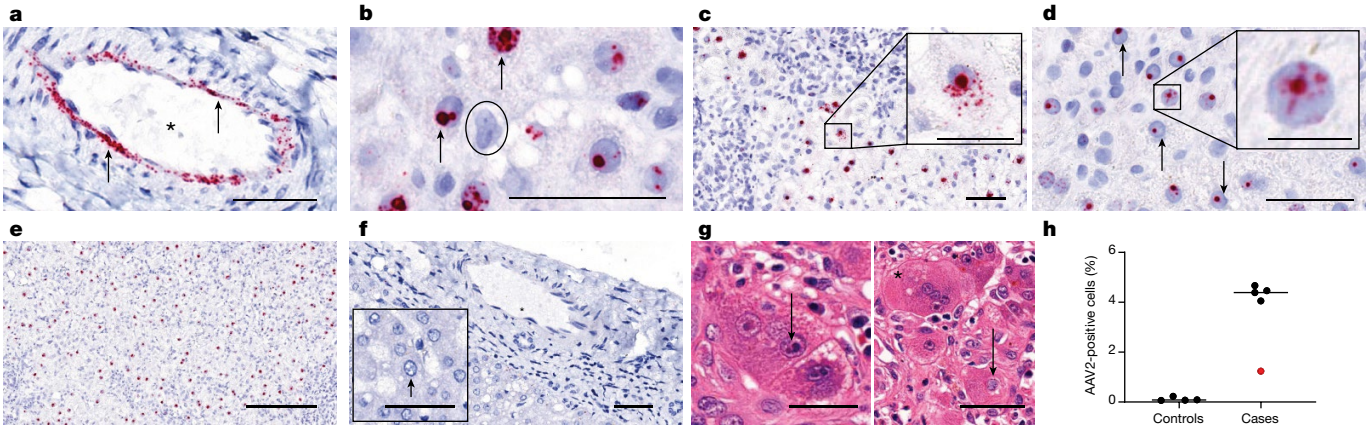

Fig. 3 | ISH of AAV2 in liver tissue. a–**g**, RNA ISH for the detection of AAV2 RNA in sections of formalin-fixed and paraffin-embedded liver tissues from children (one section per patient) with non A–E hepatitis. **a**, AAV2 RNA (red signal, indicated by an arrow) was detected in the endothelial cells of arteries in an explant liver section from patient CVR35. The vascular lumen is highlighted with by an asterisk. **b**, A positive AAV2 signal was detected in the nuclei of hepatocytes with vacuolated morphology from patient CVR4 (indicated by arrows) and in a negative cell (indicated by the circle). **c**,**d**, A liver section from patient CVR1 showed AAV2 RNA both in the nucleus and in the cytoplasm (**c**), whereas for patient CVR9 (**d**), AAV2 RNA was found only in the nucleus (indicated by arrows). **e**, A high percentage of hepatocytes with a positive signal for AAV2 was present predominantly in the nucleus of hepatocytes in the samples from patient CVR1. **f**, AAV2 was not detectable in liver sections from samples from healthy individuals in either the endothelial cells or hepatocytes. **g**, Samples from patient CVR35 showed inclusion bodies in hepatocytes. Left, small, dark basophilic intranuclear inclusions next to the nucleolus (indicated by arrows). Right, a large, pale basophilic, diffuse intranuclear inclusion body (suggestive of adenovirus infection; indicated by an arrow) next to a multinucleated giant cell in the liver (indicated by the asterisk). **h**, AAV2-positive cells were quantified using QuPath in biopsy samples from five patients with non-A–E hepatitis (cases) and from controls. Patient CVR35 (who received a liver transplant) is highlighted in red. Using the entire section, cells were segmented to identify the nuclei and cytoplasm, and the algorithm was tuned to detect red signals. All samples were analysed using the same algorithm. Scale bars, 25 µm (insets of **c**,**d**), 50 µm (**a**–**d**,**f**,**g**) or 200 µm (**e**).

activated phenotype. A $CD4^+$ T-helper cell-mediated immunopathological response triggered by exposure to AAV2 infection is highly probable, consistent with the markedly increased frequency of the MHC class II *HLA-DRB1*04:01* allele in affected children.

AAV2 is a small non-enveloped virus with a single-stranded DNA genome of around 4,675 nucleotides in length and it belongs to the species adeno-associated dependoparvovirus A (genus *Dependoparvovirus*, family *Parvoviridae*)[14]. It was first described in 1965 and infects up to 80% of the adult population. Seroconversion occurs in early childhood following respiratory infection[15,16]. In a prospective study in the United States, the earliest seroconversion to AAV2 infection occurred in a 9-month-old child, and its seroprevalence increased from 24.2% to 38.7% in 3-year-old and 5-year-old children, respectively. This age range coincides with that of the cases in this study, which suggests that illness may be related to primary infection with AAV2 rather than its reactivation. In line with this hypothesis, anti-AAV2 IgM reactivity was observed in the majority of affected children. AAV2 relies on co-infection with a helper virus for replication, most commonly HAdV or a herpesvirus. Most clinical samples taken at presentation with hepatitis were obtained more than 20 days after initial symptom onset, which could explain the absence of a helper virus in some samples and low viral loads in positive samples. In an exploratory study using NGS, we detected two candidate helper viruses at low level in the cases of hepatitis: HAdV and HHV6B (in 6 out of 9 cases and in 3 out of 9 cases, respectively). These viruses were not confirmed to be higher in cases than controls in plasma or liver samples in our larger case–control study. HHV6B was also present in two control groups that included children with severe HAdV infection and children with hepatitis of alternative aetiology. As HHV6 can establish latency and can integrate its genome into the human chromosome, it may reactivate following concomitant illness (or immunosuppression) and may represent either an opportunistic bystander or a pathogen.

We propose that AAV2 is directly implicated in the pathology of the 2022 outbreak of non-A–E hepatitis in children, which occurred following transmission as a co-infection with HAdV or less likely due to reactivation following HAdV or HHV6 infection. Our results also support an association between HLA class II haplotype and disease susceptibility. A $CD4^+$ T-cell-mediated response may direct maladaptive immunopathology mediated by T cytotoxic cells or B cells. In support of this notion, a $CD8^+$ cell-mediated response directed against the AAV2 viral capsid (VP1) in association with hepatitis was reported in early trials of AAV2 when used as a vector for gene therapy[17–19]. Hepatitis remains a common phenomenon in recipients of gene therapy vectored by AAV, and this side effect is usually treated pre-emptively with steroids before and for several weeks after the gene therapy; in rare cases, AAV-mediated gene therapy has been associated with deaths from fulminant hepatic failure[20,21]. As a result of this current study, further studies are needed investigate the association between HLA status with severe illness in gene therapy recipients. Notably, we did not find features of autoimmune hepatitis (AIH), either by serology or histology, in affected children. In a study of children from Scotland with AIH[22], the majority had evidence of seropositive disease (100% of patients with type II AIH tested positive for anti-LKM1). Furthermore, patients with AIH were older in age (median age of 11.4 years compared with 4.1 years in our cohort) and had significantly lower median alanine transaminase levels at diagnosis (444 IU per litre compared with 1,756 IU per litre). None of the AIH patients improved without treatment[22].

An alternative explanation for our findings is that AAV2 is not directly involved in pathology and is instead a biomarker of infection with HAdV. More than half of the patients with hepatitis in our study had subacute symptoms, with a median onset of 42 days before the onset of jaundice. The opportunity to detect virus by sequencing was therefore reduced, as samples were collected after this stage of illness. Furthermore, whole blood samples might have increased the sensitivity of detection, but only serum or plasma samples were available. We consider this alternative hypothesis to be less likely because we did not detect AAV2 in a control group of children with HAdV infection who had normal liver function tests. However, HAdV41 is a common cause of diarrhoea in young children[23], and co-infection of AAV2 with HAdV41 may explain early gastrointestinal symptoms in affected children. By

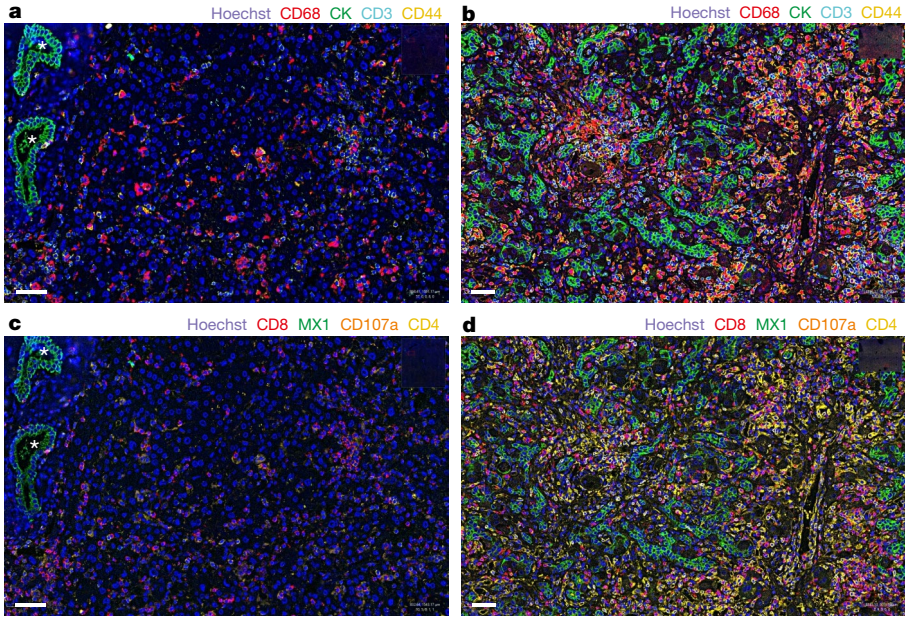

Fig. 4 | CODEX analysis of liver tissue. a–**d**, Images of liver tissue from patient CVR35 (**b**,**d**) and a liver sample from an unaffected individual (control; **a**,**c**) show differences in cellular composition (**c**,**d**). **a**, Regularly structured bile ducts in the liver biopsy from the control are highlighted by asterisks, and epithelial cells are stained green using cytokeratin (CK). Scattered macrophages (CD68, red), T cells (CD3, cyan) and activated T cells (CD44, yellow) are also present. **b**, By contrast, the explant liver from patient CVR35 shows prominent proliferation of epithelial cells throughout the liver tissue (green), with increased macrophages (red), T cells (cyan) and activated T cells (yellow). **c**, The control liver shows scattered cytotoxic T cells (CD8, red), CD107a-positive cells (brown) and CD4-positive cells (yellow) cells and low expression of the interferon-induced GTP-binding protein MX1 (green). **d**, High numbers of all cell types and high MX1 expression are observed in the explant liver from patient CVR35. One section of liver was stained per individual, and the entire area was manually outlined. Cells were segmented to identify the nuclei and cytoplasm, and the algorithm was tuned to detect the colour signal in the cells. All samples were analysed using the same algorithm for each stain. Scale bars, 50 µm.

contrast, although adenovirus-associated hepatitis has been previously described, particularly among immunocompromised individuals[24], HAdV41 has not previously been associated with severe hepatitis. In the recent outbreaks of unexplained hepatitis in children, it has been inconsistently associated[4–6,25–27].

We also investigated the possibility that the unexplained cases of hepatitis were linked to a previous illness with COVID-19. Direct SARS-CoV-2-induced liver injury is unlikely though, as few of our cases of hepatitis (3 out of 31) were positive for SARS-CoV-2 by PCR on admission to hospital, and we did not identify SARS-CoV-2 by PCR or sequencing in any of the clinical samples from cases, including liver biopsies. Furthermore, the SARS-CoV-2 seroprevalence in cases of hepatitis was lower than in the community at that time. This result is in keeping with a case–control analysis by the UK Health Security Agency[3], who found no difference in SARS-CoV-2 PCR positivity between cases of hepatitis and children presenting to emergency departments between January and June 2022. Nevertheless, we cannot at this time fully exclude a post-COVID-19 immune-mediated phenomenon, for example, a link to HLA class II type, in susceptible children.

There are several limitations to this study. First, the presence of AAV2 in cases of hepatitis but not controls in groups 1–3 may have arisen because of seasonal variation in AAV2 transmission, as some children in the control groups were sampled earlier in the year than for cases. We included a contemporaneous control group (group 4) to address this possibility. Low viral loads of AAV2 were detected in a small number of samples from the group 4 controls, which is in keeping with the presence of the circulating virus in children at the time the cases of hepatitis occurred. Second, the presence of AAV2 in the cases of hepatitis is an association and may not represent direct aetiology, and AAV2 may be a useful biomarker of recent HAdV (or less likely HHV6B) infection. We do not consider it probable that AAV2 simply represents a marker of liver damage because it was not present in cases of severe hepatitis of alternative aetiology and, significantly, we detected AAV2 in ballooned hepatocytes by ISH. The strong association of the *HLA-DRB1*04:01* allele, known to be associated with autoimmune hepatitis type 1[28] and extra-articular manifestations of rheumatoid arthritis[29], with the cases of hepatitis provides support for a large impact of host genetics on susceptibility. However, this analysis was affected by strong linkage disequilibrium, and larger studies are required to confirm a definitive association with this allele. The association between HLA status and the presence of an activated T cell infiltrate together with AAV2-infected cells in the liver is in keeping with a $CD4^+$ cell-mediated immune pathology[30]. We consider autoimmune disease to be less likely of a cause of the cases of hepatitis studied here because of the absence of autoantibodies and the absence of typical histology in liver specimens. It is also plausible that simultaneous HAdV infection with a co-infecting or reactivated AAV2 infection has resulted, for a proportion of children who are more susceptible (owing to the HLA class II allele *HLA-DRB1*04:01*), in a more severe outcome than might typically be expected for these commonly circulating viruses. Peptide mapping experiments are recommended in future studies to investigate the nature of the HLA class II-restricted T cell response.

The 2022 outbreak of AAV2-associated paediatric hepatitis that we described in this study may have arisen because of changes in exposure patterns to AAV2, HAdV and HHV6B as an indirect consequence of the COVID-19 pandemic. The circulation of common human viruses was interrupted in 2020 by the implementation of non-pharmaceutical interventions, including physical distancing and travel restrictions, instituted to mitigate SARS-CoV-2 transmission. Once restrictions were lifted, genetically susceptible children may have had a higher chance of being exposed to both HAdV and AAV2 for the first time, creating a synchronized wave of severe disease. Larger case–control studies are needed to confirm the role of AAV2 and HLA status in the aetiology

of unexplained non-A–E paediatric hepatitis. Retrospective testing of samples from sporadic cases of unexplained hepatitis in children is also needed.

Online content

Any methods, additional references, Nature Portfolio reporting summaries, source data, extended data, supplementary information, acknowledgements, peer review information; details of author contributions and competing interests; and statements of data and code availability are available at https://doi.org/10.1038/s41586-023-05948-2.

1. Marsh, K. et al. Investigation into cases of hepatitis of unknown aetiology among young children, Scotland, 1 January 2022 to 12 April 2022. *Euro Surveill.* https://doi.org/10.2807/1560-7917.ES.2022.27.15.2200318 (2022).
2. Severe acute hepatitis of unknown aetiology in children—multi-country. *World Health Organization* (12 July 2022); https://www.who.int/emergencies/disease-outbreak-news/item/2022-DON400.
3. *Investigation into Acute Hepatitis of Unknown Aetiology in Children in England. Technical Briefing 4* (UK Health Security Agency, 2022).
4. Gutierrez Sanchez, L. H. et al. A case series of children with acute hepatitis and human adenovirus infection. *N. Engl. J. Med.* https://doi.org/10.1056/NEJMoa2206294 (2022).
5. Karpen, S. J. Acute hepatitis in children in 2022—human adenovirus 41? *N. Engl. J. Med*. https://doi.org/10.1056/NEJMe2208409 (2022).
6. Kelgeri, C. et al. Clinical spectrum of children with acute hepatitis of unknown cause. *N. Engl. J. Med.* https://doi.org/10.1056/NEJMoa2206704 (2022).
7. Dunning, J. W. et al. Open source clinical science for emerging infections. *Lancet Infect. Dis.* **14**, 8–9 (2014).
8. Knodell, R. G. et al. Formulation and application of a numerical scoring system for assessing histological activity in asymptomatic chronic active hepatitis. *Hepatology* **1**, 431–435 (1981).
9. Krishna, M. Histological grading and staging of chronic hepatitis. *Clin. Liver Dis.* **17**, 222–226 (2021).
10. Hsu, H. L. et al. Structural characterization of a novel human adeno-associated virus capsid with neurotropic properties. *Nat. Commun.* **11**, 3279 (2020).
11. Enhanced Surveillance of Covid-19 in Scotland (Population-based seroprevalence)—5 Week Rolling Estimate. *Public Health Scotland* (1 June 2022); https://publichealthscotland.scot/publications/enhanced-surveillance-of-covid-19-in-scotland/enhanced-surveillance-of-covid-19-in-scotland-population-based-seroprevalence-surveillance-1-june-2022/dashboard/.
12. Rodriguez-Inigo, E. et al. Percentage of hepatitis C virus-infected hepatocytes is a better predictor of response than serum viremia levels. *J. Mol. Diagn.* **7**, 535–543 (2005).
13. Tomlinson, J. E. et al. Tropism, pathology, and transmission of equine parvovirus-hepatitis. *Emerg. Microbes Infect.* **9**, 651–663 (2020).
14. Srivastava, A., Lusby, E. W. & Berns, K. I. Nucleotide sequence and organization of the adeno-associated virus 2 genome. *J. Virol.* **45**, 555–564 (1983).
15. Atchison, R. W., Casto, B. C. & Hammon, W. M. Adenovirus-associated defective virus particles. *Science* **149**, 754–756 (1965).
16. Li, C. et al. Neutralizing antibodies against adeno-associated virus examined prospectively in pediatric patients with hemophilia. *Gene Ther.* **19**, 288–294 (2012).
17. Martino, A. T. et al. Engineered AAV vector minimizes in vivo targeting of transduced hepatocytes by capsid-specific $CD8^+$ T cells. *Blood* **121**, 2224–2233 (2013).
18. Manno, C. S. et al. Successful transduction of liver in hemophilia by AAV-factor IX and limitations imposed by the host immune response. *Nat. Med.* **12**, 342–347 (2006).
19. Mingozzi, F. et al. $CD8^+$ T-cell responses to adeno-associated virus capsid in humans. *Nat. Med.* **13**, 419–422 (2007).
20. Ertl, H. C. J. Immunogenicity and toxicity of AAV gene therapy. *Front. Immunol.* **13**, 975803 (2022).
21. Chowdary, P. et al. Phase 1–2 trial of AAVS3 gene therapy in patients with hemophilia B. *N. Engl. J. Med.* **387**, 237–247 (2022).
22. Sebode, M., Weiler-Normann, C., Liwinski, T. & Schramm, C. Autoantibodies in autoimmune liver disease—clinical and diagnostic relevance. *Front. Immunol.* **9**, 609 (2018).
23. Rafie, K. et al. The structure of enteric human adenovirus 41—a leading cause of diarrhea in children. *Sci. Adv.* **7**, eabe0974 (2021).
24. Echavarria, M. Adenoviruses in immunocompromised hosts. *Clin. Microbiol. Rev.* **21**, 704–715 (2008).
25. Baker, J. M. et al. Acute hepatitis and adenovirus infection among children—Alabama, October 2021–February 2022. *MMWR Morb. Mortal. Wkly Rep.* **71**, 638–640 (2022).
26. Cooper, S. et al. Long COVID-19 liver manifestation in children. *J. Pediatr. Gastroenterol. Nutr.* https://doi.org/10.1097/MPG.0000000000003521 (2022).
27. Deep, A., Grammatikopoulos, T., Heaton, N., Verma, A. & Dhawan, A. Outbreak of hepatitis in children: clinical course of children with acute liver failure admitted to the intensive care unit. *Intensive Care Med.* https://doi.org/10.1007/s00134-022-06765-3 (2022).
28. van Gerven, N. M. et al. HLA-DRB1*03:01 and HLA-DRB1*04:01 modify the presentation and outcome in autoimmune hepatitis type-1. *Genes Immun.* **16**, 247–252 (2015).
29. Lanchbury, J. S. et al. Strong primary selection for the Dw4 subtype of DR4 accounts for the HLA-DQw7 association with Felty's syndrome. *Hum. Immunol.* **32**, 56–64 (1991).
30. Gay, D. et al. Functional interaction between human T-cell protein CD4 and the major histocompatibility complex HLA-DR antigen. *Nature* **328**, 626–629 (1987).

DIAMONDS Consortium

Michael Levin[13], Aubrey Cunnington[13], Jethro Herberg[13], Myrsini Kaforou[13], Victoria Wright[13], Evangelos Bellos[13], Claire Broderick[13], Samuel Channon-Wells[13], Samantha Cooray[13], Tisham De[13], Giselle D'Souza[13], Leire Estramiana Elorrieta[13], Diego Estrada-Rivadeneyra[13], Rachel Galassini[13], Dominic Habgood-Coote[13], Shea Hamilton[13], Heather Jackson[13], James Kavanagh[13], Mahdi Moradi Marjaneh[13], Stephanie Menikou[13], Samuel Nichols[13], Ruud Nijman[13], Harsita Patel[13], Ivana Pennisi[13], Oliver Powell[13], Ruth Reid[13], Priyen Shah[13], Ortensia Vito[13], Elizabeth Whittaker[13], Clare Wilson[13], Rebecca Womersley[13], Amina Abdulla[19], Sarah Darnell[19], Sobia Mustafa[19], Pantelis Georgiou[20], Jesus-Rodriguez Manzano[21], Nicolas Moser[20], Ivana Pennisi[3], Michael Carter[22,23], Shane Tibby[22,23], Jonathan Cohen[22], Francesca Davis[22], Julia Kenny[22], Paul Wellman[22], Marie White[22], Matthew Fish[24], Aislinn Jennings[25], Manu Shankar-Hari[24,25], Katy Fidler[26], Dan Agranoff[27], Vivien Richmond[26,28], Mathew Seal[27], Saul Faust[29], Dan Owen[29], Ruth Ensom[30], Sarah McKay[30], Diana Mondo[31], Mariya Shaji[31], Rachel Schranz[31], Prita Rughnani[32,33,34], Amutha Anpananthar[32,33,34], Susan Liebeschuetz[33], Anna Riddell[32], Nosheen Khalid[32,34], Ivone Lancoma Malcolm[34], Teresa Simagan[34], Mark Peters[35,36], Alasdair Bamford[35,36], Lauran O'Neill[35], Nazima Pathan[37,38], Esther Daubney[37], Deborah White[37], Melissa Heightman[39], Sarah Eisen[39], Terry Segal[39], Lucy Wellings[39], Simon B. Drysdale[40], Nicole Branch[40], Lisa Hamzah[40], Heather Jarman[40], Maggie Nyirenda[3,41], Lisa Capozzi[41], Emma Gardiner[41], Robert Moots[42], Magda Nasher[43], Anita Hanson[43], Michelle Linforth[42], Sean O'Riordan[44], Donna Ellis[44], Akash Deep[45], Ivan Caro[45], Fiona Shackley[46], Arianna Bellini[46], Stuart Gormley[46], Samira Neshat[47], Barnaby J. Scholefield[48], Ceri Robbins[48], Helen Winmill[48], Stéphane C. Paulus[49,50,51], Andrew J. Pollard[49,50,51,52], Mark Anthony[49], Sarah Hopton[49], Danielle Miller[49], Zoe Oliver[49], Sally Beer[49], Bryony Ward[49], Shrijana Shrestha[53], Andrew J. Pollard[52,54], Meeru Gurung[53], Puja Amatya[53], Bhishma Pokhrel[53], Sanjeev Man Bijukchhe[53], Tim Lubinda[54], Sarah Kelly[54], Peter O'Reilly[54], Federico Martinón-Torres[55,56], Antonio Salas[55,56,57], Fernando Álvez González[55,56], Xabier Bello[55,56,58], Mirian Ben García[55,56], Sandra Carnota[55,56], Miriam Cebey-López[55,56], María José Curras-Tuala[55,56,57], Carlos Durán Suárez[55,56], Luisa García Vicente[55,56], Alberto Gómez-Carballa[55,56,57], Jose Gómez Rial[55,56], Pilar Leboráns Iglesias[55,56], Federico Martinón-Torres[55,56], Nazareth Martinón-Torres[55,56], José María Martinón Sánchez[55,56], Belén Mosquera Pérez[55,56], Jacobo Pardo-Seco[55,56,57], Lidia Piñeiro Rodríguez[55,56], Sara Pischedda[55,56,57], Sara Rey Vázquez[55,56], Irene Rivero Calle[55,56], Carmen Rodríguez-Tenreiro[55,56], Lorenzo Redondo-Collazo[55,56], Miguel Sadiki Ora[55,56], Antonio Salas[55,56,57], Sonia Serén Fernández[55,56], Cristina Serén Trasorras[55,56], Marisol Vilas Iglesias[55,56], Enitan D. Carrol[59,60], Elizabeth Cocklin[59], Aakash Khanijau[59], Rebecca Lenihan[59], Nadia Lewis-Burke[59], Karen Newall[60], Sam Romaine[59], Maria Tsolia[61], Irini Eleftheriou[61], Nikos Spyridis[61], Maria Tambouratzi[61], Despoina Maritsi[61], Antonios Marmarinos[61], Marietta Xagorari[61], Lourida Panagiota[62], Pefanis Aggelos[62], Akinosoglou Karolina[63], Gogos Charalambos[63], Maragos Markos[63], Voulgarelis Michalis[64], Stergiou Ioanna[64], Marieke Emonts[65,66,67], Emma Lim[66,67,68], John Isaacs[65], Kathryn Bell[69], Stephen Crulley[69], Daniel Fabian[69], Evelyn Thomson[69], Diane Wallia[69], Caroline Miller[69], Ashley Bell[69], Fabian J. S. van der Velden[65,66], Geoff Shenton[70], Ashley Price[71,72], Owen Treloar[65,66], Daisy Thomas[65,66], Pablo Rojo[73,74], Cristina Epalza[73,75], Serena Villaverde[73], Sonia Márquez[75], Manuel Gijón[75], Fátima Machín[75], Laura Cabello[75], Irene Hernández[75], Lourdes Gutiérrez[75], Ángela Manzanares[73], T. W. Taco Kuijpers[76,77], M. Martijn van de Kuip[76], A. M. Marceline van Furth[76], J. M. Merlijn van den Berg[76], Giske Biesbroek[76], Floris Verkuil[76], Carlijn C. W. van der Zee[76], Dasja Pajkrt[76], Michael Boele van Hensbroek[76], Dieneke Schonenberg[76], Mariken Gruppen[76], Sietse Nagelkerke[76,77], Machiel H. Jansen[76], Ines Goetschalckx[77], Lorenza Romani[78], Maia De Luca[78], Sara Chiurchiù[78], Martina Di Giuseppe[78], Clementien L. Vermont[79], Henriëtte A. Moll[80], Dorine M. Borensztajn[80], Nienke N. Hagedoorn[80], Chantal Tan[80], Joany Zachariasse[80], Medical students[80], W. Dik[81], Ching-Fen Kitty Shen[82], Dace Zavadska[83,84], Sniedze Laivacuma[83,85], Aleksandra Rudzate[83,84], Diana Stoldere[83,84], Arta Barzdina[83,84], Elza Barzdina[83,84], Sniedze Laivacuma[83,85], Monta Madelane[83,85], Dagne Gravele[84], Dace Svile[84], Romain Basmaci[86,87], Noémie Lachaume[86], Pauline Bories[86], Raja Ben Tkhayat[86], Laura Chériaux[86], Juraté Davoust[86], Kim-Thanh Ong[86], Marie Cotillon[86], Thibault de Groc[86], Sébastien Le[86], Nathalie Vergnault[86], Hélène Sée[86], Laure Cohen[86], Alice de Tugny[86], Nevena Danekova[86], Marine Mommert-Tripon[88], Karen Brengel-Pesce[88], Marko Pokorn[89,90,91], Mojca Kolnik[90], Tadej Avčin[90,91], Tanja Avramoska[90], Natalija Bahovec[89], Petra Bogovič[89], Lidija Kitanovski[90,91], Mirijam Nahtigal[89], Lea Papst[89], Tina Plankar Srovin[89], Franc Strle[89,90], Anja Srpčič[90], Katarina Vincek[89], Michiel van der Flier[92,93], Wim J. E. Tissing[94], Roelie M. Wösten-van Asperen[94], Sebastiaan J. Vastert[95], Daniel C. Vijlbrief[96], Louis J. Bont[92,93], Tom F. W. Wolfs[92,93], Coco R. Beudeker[92,93], Philipp Agyeman[97], Luregn Schlapbach[98,99], Christoph Aebi[97], Mariama Usman[97], Stefanie Schlüchter[97], Verena Wyss[97], Nina Schöbi[97], Elisa Zimmermann[98], Marion Meier[98], Kathrin Weber[98], Philipp Agyeman[98], Luregn J. Schlapbach[100,101], Eric Giannoni[102,103], Martin Stocker[104], Klara M. Posfay-Barbe[105], Ulrich Heininger[106], Sara Bernhard-Stirnemann[107], Anita Niederer-Loher[108], Christian Kahlert[108], Giancarlo Natalucci[109], Christa Relly[110], Thomas Riedel[111], Christoph Aebi[98], Christoph Berger[110], Colin Fink[112], Marie Voice[112], Leo Calvo-Bado[112], Michael Steele[112], Jennifer Holden[112], Benjamin Evans[112], Jake Stevens[112], Peter Matthews[112], Kyle Billing[112], Werner Zenz[113], Alexander Binder[113], Benno Kohlmaier[113], Daniela S. Kohlfürst[113], Nina A. Schweintzger[113], Christoph Zurl[113], Susanne Hösele[113], Manuel Leitner[113], Lena Pölz[113], Alexandra Rusu[114], Glorija Rajic[113], Bianca Stoiser[113], Martina Strempfl[113], Manfred G. Sagmeister[113], Sebastian Bauchinger[113], Martin Benesch[115], Astrid Ceolotto[113], Ernst Eber[114], Siegfried Gallistl[113], Harald Haidl[113], Almuthe Hauer[113], Christa Hude[113], Andreas Kapper[116], Markus Keldorfer[117], Sabine Löffler[117], Tobias Niedrist[118], Heidemarie Pilch[117], Andreas Pfleger[114], Klaus Pfurtscheller[116], Siegfried Rödl[116], Andrea Skrabl-Baumgartner[113], Volker Strenger[115], Elmar Wallner[119], Dennie Tempel[120], Danielle van Keulen[120], Annelieke M. Strijbosch[120], Maike K. Tauchert[121], Ulrich von Both[122,123], Laura Kolberg[122], Patricia Schmied[122], Irene Alba-Alejandre[124], Katharina Danhauser[125], Nikolaus Haas[126], Florian Hoffmann[127], Matthias Griese[128], Tobias Feuchtinger[129], Sabrina Juranek[130], Matthias Kappler[128], Eberhard Lurz[131], Esther Maier[130], Karl Reiter[127], Carola Schoen[127], Sebastian Schroepf[132], Shunmay Yeung[18,133], Manuel Dewez[18], David Bath[134], Elizabeth Fitchett[18], Fiona Cresswell[18], Saidykhan Momodou[135], Effua Usuf[135], Ebrahim Ndure[135], Kalifa Bojang[135], Anna Roca[135] & Isatou Sarr[135]

[19]Children's Clinical Research Unit, St Mary's Hospital, London, UK. [20]Department of Electrical and Electronic Engineering, Imperial College London, South Kensington Campus, London, UK. [21]Imperial College London, Department of Infectious Disease, Section of Adult Infectious Disease, Imperial College London, Hammersmith Campus, London, UK. [22]Evelina London Children's Hospital, Guy's and St Thomas' NHS Foundation Trust, London, UK. [23]Department of Women and Children's Health, School of Life Course Sciences, King's College London, London, UK. [24]Department of Infectious Diseases, School of Immunology and Microbial Sciences, King's College London, London, UK. [25]Department of Intensive Care Medicine, Guy's and St Thomas' NHS Foundation Trust, London, UK. [26]Royal Alexandra Children's Hospital, University Hospitals Sussex, Brighton, UK. [27]Department of Infectious Diseases, University Hospitals Sussex, Brighton, UK. [28]Research Nurse Team, University Hospitals Sussex, Brighton, UK. [29]NIHR Southampton Clinical Research Facility, University Hospital Southampton NHS Foundation Trust and University of Southampton, Southampton, UK. [30]NIHR Southampton Clinical Research Facility, University Hospital Southampton NHS Foundation Trust, Southampton, UK. [31]Department of R&D, University Hospital Southampton NHS Foundation Trust, Southampton, UK. [32]Royal London Hospital, London, UK. [33]Newham University Hospital, London, UK. [34]Whipps Cross University Hospital, London, UK. [35]Great Ormond Street Hospital, London, UK. [36]UCL Great Ormond Street Institute of Child Health, London, UK. [37]Addenbrooke's Hospital, Cambridge, UK. [38]Department of Paediatrics, University of Cambridge, Cambridge, UK. [39]University College London Hospital, London, UK. [40]St George's Hospital, London, UK. [41]University Hospital Lewisham, London, UK. [42]Aintree University Hospital, Lower Lane, Liverpool, UK. [43]Royal Liverpool Hospital, Prescot St, Liverpool, UK. [44]Leeds Children's Hospital, Leeds, UK. [45]Kings College Hospital, Denmark Hill, London, UK. [46]Sheffield Children's Hospital, Broomhall, Sheffield, UK. [47]Leicester General Hospital, Leicester, UK. [48]Birmingham Children's Hospital, Steelhouse Lane, Birmingham, UK. [49]John Radcliffe Hospital, Oxford University Hospitals NHS Foundation Trust, Oxford, UK. [50]Department of Paediatrics, University of Oxford, Oxford, UK. [51]Oxford Vaccine Group, University of Oxford, Oxford, UK. [52]NIHR Oxford Biomedical Research Centre, Oxford, UK. [53]Paediatric Research Unit, Patan Academy of Health Sciences, Kathmandu, Nepal. [54]Oxford Vaccine Group, Department of Paediatrics, University of Oxford, Oxford, UK. [55]Translational Pediatrics and Infectious Diseases, Pediatrics Department, Hospital Clínico Universitario de Santiago, Santiago de Compostela, Galicia, Spain. [56]GENVIP Research Group, Instituto de Investigación Sanitaria de Santiago, Universidad de Santiago de Compostela, Galicia, Spain. [57]Unidade de Xenética, Departamento de Anatomía Patolóxica e Ciencias Forenses, Instituto de Ciencias Forenses, Facultade de Medicina, Universidade de Santiago de Compostela, and GenPop Research Group, Instituto de Investigaciones Sanitarias (IDIS), Hospital Clínico Universitario de Santiago, Galicia, Spain. [58]Fundación Pública Galega de Medicina Xenómica, Servizo Galego de Saúde (SERGAS), Instituto de Investigaciones Sanitarias (IDIS), and Grupo de Medicina Xenómica, Centro de Investigación Biomédica en Red de Enfermedades Raras (CIBERER), Universidade de Santiago de Compostela (USC), Santiago de Compostela, Spain. [59]Department of Clinical Infection, Microbiology and Immunology, University of Liverpool Institute of Infection, Veterinary and Ecological Sciences, Liverpool, UK. [60]Department of Infectious Diseases, Alder Hey Children's Hospital, Liverpool, UK. [61]2nd Department of Pediatrics, National and Kapodistrian University of Athens (NKUA), Children's Hospital "P, and A. Kyriakou", Athens, Greece. [62]1st Department of Infectious Diseases, Sotiria General Hospital, Athens, Greece. [63]Pathology Department, University of Patras, General Hospital "Panagia i Voithia", Patras, Greece. [64]Pathophysiology Department, Medical Faculty, National and Kapodistrian, Laiko General Hospital–University of Athens (NKUA), Athens, Greece. [65]Translational and Clinical Research Institute, Newcastle University, Newcastle upon Tyne, UK. [66]Great North Children's Hospital, Paediatric Immunology, Infectious Diseases and Allergy, Newcastle upon Tyne Hospitals NHS Foundation Trust, Newcastle upon Tyne, UK. [67]NIHR Newcastle Biomedical Research Centre, Newcastle upon Tyne Hospitals NHS Trust and Newcastle University, Newcastle upon Tyne, UK. [68]Population Health Sciences Institute, Newcastle University, Newcastle upon Tyne, UK. [69]Great North Children's Hospital Research Unit, Newcastle upon Tyne, UK. [70]Great North Children's Hospital, Paediatric Oncology, Newcastle upon Tyne Hospitals NHS Foundation Trust, Newcastle upon Tyne, UK. [71]Department of Infection and Tropical Medicine, Newcastle upon Tyne Hospitals NHS Foundation Trust, Newcastle upon Tyne, UK. [72]NIHR Newcastle In Vitro Diagnostics Co-operative (Newcastle MIC), Newcastle upon Tyne, UK. [73]Servicio Madrileño de Salud (SERMAS), Pediatric Infectious Diseases Unit, Department of Pediatrics, Hospital Universitario 12 de Octubre, Madrid, Spain. [74]Department of Pediatrics, Faculty of Medicine, Universidad Complutense de Madrid, Madrid, Spain. [75]Fundación Biomédica del Hospital Universitario 12 de Octubre (FIB-H12O), Unidad Pediátrica de Investigación y Ensayos Clínicos (UPIC), Hospital Universitario 12 de Octubre, Instituto de Investigación Sanitaria Hospital 12 de Octubre (i+12), Madrid, Spain. [76]Amsterdam UMC, Emma Children's Hospital, Department of Pediatric Immunology, Rheumatology and Infectious Disease, University of Amsterdam, Amsterdam, The Netherlands. [77]Sanquin, Department of Molecular Hematology, University Medical Center, Amsterdam, The Netherlands. [78]Infectious Disease Unit, Academic Department of Pediatrics, Bambino Gesù Children's Hospital, IRCCS, Rome, Italy. [79]Department of Paediatric Infectious Diseases and Immunology, Erasmus MC-Sophia Children's Hospital, Rotterdam, The Netherlands. [80]Department of General Paediatrics, Erasmus MC-Sophia Children's Hospital, Rotterdam, The Netherlands. [81]Department of Immunology, Erasmus MC, Rotterdam, The Netherlands. [82]Division of Infectious Disease, Department of Pediatrics, National Cheng Kung University Tainan, Tainan, Taiwan. [83]Riga Stradins University, Riga, Latvia. [84]Children Clinical University Hospital, Riga, Latvia. [85]Riga East Clinical University Hospital, Riga, Latvia. [86]Service de Pédiatrie-Urgences, AP-HP, Hôpital Louis-Mourier, Colombes, France. [87]Université Paris Cité, Inserm, IAME, Paris, France. [88]BioMérieux–Open Innovation and Partnerships Department, Lyon, France. [89]Department of Infectious diseases, University Medical Centre Ljubljana, Ljubljana, Slovenia. [90]University Children's Hospital, University Medical Centre Ljubljana, Ljubljana, Slovenia. [91]Faculty of Medicine, University of Ljubljana, Ljubljana, Slovenia. [92]Pediatric Infectious Diseases and Immunology, University Medical Center Utrecht, Utrecht, The Netherlands. [93]Princess Maxima Center for Pediatric Oncology, Utrecht, The Netherlands. [94]Pediatric Intensive Care Unit, University Medical Center Utrecht,

Utrecht, The Netherlands. [95]Pediatric Rheumatology, University Medical Center Utrecht, Utrecht, The Netherlands. [96]Pediatric Neonatal Intensive Care, Wilhelmina Children's Hospital, University Medical Center Utrecht, Utrecht, The Netherlands. [97]Department of Pediatrics, Inselspital, Bern University Hospital, University of Bern, Bern, Switzerland. [98]Department of Intensive Care and Neonatology, and Children's Research Center, University Children's Hospital Zurich, Zurich, Switzerland. [99]Child Health Research Centre, The University of Queensland, Brisbane, Queesnland, Australia. [100]Department of Intensive Care and Neonatology, and Children's Research Center, University Children's Hospital Zurich, Zurich, Switzerland. [101]Child Health Research Centre, The University of Queensland, Brisbane, Queensland, Australia. [102]Clinic of Neonatology, Department Mother-Woman-Child, Lausanne University Hospital and University of Lausanne, Lausanne, Switzerland. [103]Infectious Diseases Service, Department of Medicine, Lausanne University Hospital and University of Lausanne, Lausanne, Switzerland. [104]Department of Pediatrics, Children's Hospital Lucerne, Lucerne, Switzerland. [105]Pediatric Infectious Diseases Unit, Children's Hospital of Geneva, University Hospitals of Geneva, Geneva, Switzerland. [106]Infectious Diseases and Vaccinology, University of Basel Children's Hospital, Basel, Switzerland. [107]Children's Hospital Aarau, Aarau, Switzerland. [108]Division of Infectious Diseases and Hospital Epidemiology, Children's Hospital of Eastern Switzerland St Gallen, St Gallen, Switzerland. [109]Department of Neonatology, University Hospital Zurich, Zurich, Switzerland. [110]Division of Infectious Diseases and Hospital Epidemiology, and Children's Research Center, University Children's Hospital Zurich, Zurich, Switzerland. [111]Children's Hospital Chur, Chur, Switzerland. [112]Micropathology, The Venture Center, University of Warwick Science Park, Coventry, UK. [113]Department of Pediatrics and Adolescent Medicine, Division of General Pediatrics, Medical University of Graz, Graz, Austria. [114]Department of Pediatric Pulmonology, Medical University of Graz, Graz, Austria. [115]Department of Pediatric Hematooncology, Medical University of Graz, Graz, Austria. [116]Paediatric Intensive Care Unit, Medical University of Graz, Graz, Austria. [117]University Clinic of Pediatrics and Adolescent Medicine Graz, Medical University Graz, Graz, Austria. [118]Clinical Institute of Medical and Chemical Laboratory Diagnostics, Medical University Graz, Graz, Austria. [119]Department of Internal Medicine, State Hospital Graz II, Location West, Graz, Austria. [120]SkylineDx, Rotterdam, The Netherlands. [121]Biobanking and BioMolecular Resources Research Infrastructure–European Research Infrastructure Consortium (BBMRI-ERIC), Graz, Austria. [122]Division of Pediatric Infectious Diseases, Department of Pediatrics, Dr von Hauner Children's Hospital, University Hospital, LMU Munich, Munich, Germany. [123]German Center for Infection Research (DZIF), Partner Site Munich, Munich, Germany. [124]Department of Gynecology and Obstetrics, University Hospital, LMU Munich, Munich, Germany. [125]Division of Pediatric Rheumatology, Department of Pediatrics, Dr von Hauner Children's Hospital, University Hospital, LMU Munich, Munich, Germany. [126]Department of Pediatric Cardiology and Pediatric Intensive Care, University Hospital, LMU Munich, Munich, Germany. [127]Paediatric Intensive Care Unit, Department of Pediatrics, Dr von Hauner Children's Hospital, University Hospital, LMU Munich, Munich, Germany. [128]Division of Pediatric Pulmonology, Department of Pediatrics, Dr von Hauner Children's Hospital, University Hospital, LMU Munich, Munich, Germany. [129]Division of Pediatric Haematology and Oncology, Department of Pediatrics, Dr von Hauner Children's Hospital, University Hospital, LMU Munich, Munich, Germany. [130]Division of General Pediatrics, Department of Pediatrics, Dr von Hauner Children's Hospital, University Hospital, LMU Munich, Munich, Germany. [131]Division of Pediatric Gastroenterology, Department of Pediatrics, Dr von Hauner Children's Hospital, University Hospital, LMU Munich, Munich, Germany. [132]Neonatal Intensive Care Unit, Department of Pediatrics, Dr von Hauner Children's Hospital, University Hospital, LMU Munich, Munich, Germany. [133]Department of Paediatrics, St Mary's Imperial College Hospital, London, UK. [134]Department of Global Health and Development, Faculty of Public Health and Policy, London School of Hygiene and Tropical Medicine, London, UK. [135]Medical Research Council Unit, The Gambia at LSHTM, Banjul, The Gambia.

ISARIC4C Investigators

J. Kenneth Baillie[3,14,207], Malcolm G. Semple[136,137], Gail Carson[138], Peter J. M. Openshaw[139,140], Jake Dunning[139,141], Laura Merson[138], Clark D. Russell[142], David Dorward[143], Maria Zambon[141], Meera Chand[12], Richard S. Tedder[144,145,146], Saye Khoo[147], Lance C. W. Turtle[136,148], Tom Solomon[136,149], Samreen Ijaz[141], Tom Fletcher[150], Massimo Palmarini[1], Antonia Ho[1,206], Emma C. Thomson[1], Nicholas Price[151,152], Judith Breuer[153], Thushan de Silva[154], Chloe Donohue[155], Hayley Hardwick[136], Wilna Oosthuyzen[3], Miranda Odam[3], Primrose Chikowore[3], Lauren Obosi[3], Sara Clohisey[3], Andrew Law[3], Lucy Norris[156], Sarah Tait[6], Murray Wham[3], Richard Clark[157], Audrey Coutts[157], Lorna Donnelly[157], Angie Fawkes[157], Tammy Gilchrist[157], Katarzyna Hafezi[157], Louise MacGillivray[157], Alan Maclean[157], Sarah McCafferty[157], Kirstie Morrice[157], Lee Murphy[157], Nicola Wrobel[157], Sarah E. McDonald[1], Victoria Shaw[158], Katie A. Ahmed[158], Jane A. Armstrong[159], Lauren Lett[160], Paul Henderson[161], Louisa Pollock[162], Shyla Kishore[163], Helen Brotherton[164], Lawrence Armstrong[165], Andrew Mitra[166], Anna Dall[167], Kristyna Bohmova[168], Sheena Logan[168], Louise Gannon[169,170], Ken Agwuh[171], Srikanth Chukkambotla[172], Ingrid DuRand[173], Duncan Fullerton[174], Sanjeev Gar[175], Clive Graham[176], Tassos Grammatikopoulos[177,178], Stuart Hartshorn[179], Luke Hodgson[180], Paul Jennings[181], George Koshy[182], Tamas Leiner[182], James Limb[183], Jeff Little[184], Sheena Logan[184], Elijah Matovu[174], Fiona McGill[185], Craig Morris[186], John Morrice[187], David Price[188], Henrik Reschreiter[189], Tim Reynolds[186], Paul Whittaker[190], Thomas Jordan[164], Rachel Tayler[191], Clare Irving[192], Katherine Jack[161], Maxine Ramsay[161], Margaret Millar[161], Barry Milligan[193], Naomi Hickey[193], Maggie Connon[163], Catriona Ward[163], Laura Beveridge[187], Susan MacFarlane[169,170], Karen Leitch[164], Claire Bell[194], Lauren Finlayson[167], Joy Dawson[167], Janie Candlish[166], Laura McGenily[168], Tara Roome[179], Cynthia Diaba[195], Jasmine Player[196], Natassia Powell[197], Ruth Howman[179], Sara Burling[179], Sharon Floyd[180], Sarah Farmer[171], Susie Ferguson[198], Susan Hope[199], Lucy Rubick[189], Rachel Swingler[200], Emma Collins[201], Collette Spencer[185], Amaryl Jones[174], Barbara Wilson[202], Diane Armstrong[203], Mark Birt[204], Holly Dickinson[186], Rosemary Harper[203], Darran Martin[205], Amy Roff[189] & Sarah Mills[189]

[136]NIHR Health Protection Research Unit, Institute of Infection, Veterinary and Ecological Sciences, Faculty of Health and Life Sciences, University of Liverpool, Liverpool, UK. [137]Respiratory Medicine, Alder Hey Children's Hospital, Institute in The Park, University of Liverpool, Alder Hey Children's Hospital, Liverpool, UK. [138]ISARIC Global Support Centre, Centre for Tropical Medicine and Global Health, Nuffield Department of Medicine, University of Oxford, Oxford, UK. [139]National Heart and Lung Institute, Imperial College London, London, UK. [140]Imperial College Healthcare NHS Trust London, London, UK. [141]National Infection Service, Public Health England, London, UK. [142]Centre for Inflammation Research, The Queen's Medical Research Institute, University of Edinburgh, Edinburgh, UK. [143]Edinburgh Pathology, University of Edinburgh, Edinburgh, UK. [144]Blood Borne Virus Unit, Virus Reference Department, National Infection Service, Public Health England, London, UK. [145]Transfusion Microbiology, National Health Service Blood and Transplant, London, UK. [146]Department of Medicine, Imperial College London, London, UK. [147]Department of Pharmacology, University of Liverpool, Liverpool, UK. [148]Tropical and Infectious Disease Unit, Royal Liverpool University Hospital, Liverpool, UK. [149]Walton Centre NHS Foundation Trust, Liverpool, UK. [150]Liverpool School of Tropical Medicine, Liverpool, UK. [151]Centre for Clinical Infection and Diagnostics Research, Department of Infectious Diseases, School of Immunology and Microbial Sciences, King's College London, London, UK. [152]Department of Infectious Diseases, Guy's and St Thomas' NHS Foundation Trust, London, UK. [153]Division of Infection and Immunity, University College London and Great Ormond Street Hospital, London, UK. [154]The Florey Institute for Host–Pathogen Interactions, Department of Infection, Immunity and Cardiovascular Disease, University of Sheffield, Sheffield, UK. [155]Liverpool Clinical Trials Centre, University of Liverpool, Liverpool, UK. [156]EPCC, University of Edinburgh, Edinburgh, UK. [157]Edinburgh Clinical Research Facility, University of Edinburgh, Edinburgh, UK. [158]Institute of Translational Medicine, University of Liverpool, Liverpool, UK. [159]Sheffield Teaching Hospitals, Sheffield, UK. [160]University of Liverpool, Liverpool, UK. [161]Royal Hospital for Children and Young People, Edinburgh, UK. [162]Department of Paediatric Infectious Diseases and Immunology, Royal Hospital for Children, Glasgow, UK. [163]Royal Aberdeen Children's Hospital, Aberdeen, UK. [164]University Hospital Wishaw, North Lanarkshire, UK. [165]Crosshouse and Ayr Hospital, Kilmarnock, UK. [166]Dumfries and Galloway Royal Infirmary, Dumfries, UK. [167]Borders General Hospital, Melrose, UK. [168]Forth Valley Royal Hospital, Larbert, UK. [169]Tayside Children's Hospital, Ninewells Hospital, NHS Tayside, Dundee, UK. [170]Ninewells Hospital, NHS Tayside, Dundee, UK. [171]Doncaster and Bassetlaw Teaching Hospitals NHS Foundation Trust, Doncaster, UK NHS Foundation Trust, Doncaster, UK. [172]Burnley General Teaching Hospital, Burnley, UK. [173]Hereford County Hospital, Hereford, UK. [174]Leighton Hospital, Leighton, UK. [175]Walsall Healthcare NHS Trust, Walsall, UK. [176]Cumberland Infirmary, Cumberland, UK. [177]Paediatric Liver, GI & Nutrition Centre and MowatLabs, King's College Hospital, London, UK. [178]Institute of Liver Studies, King's College London, London, UK. [179]Birmingham Women's Children's Hospital, Birmingham, UK. [180]St Richards' Hospital, Chichester, UK. [181]Airedale General Hospital, Keighley, UK. [182]Hinchingbrooke Hospital, Huntingdon, UK. [183]Darlington Memorial Hospital, Darlington, UK. [184]Warrington Hospital, Kilmarnock, UK. [185]Leeds Teaching Hospitals NHS Trust, Leeds, UK. [186]Queens Hospital Burton, Burton-on-Trent, UK. [187]Queen Margaret Hospital, Dunfermline, UK. [188]Royal Victoria Infirmary, Newcastle upon Tyne, UK. [189]Poole University Hospital, Dorset, UK. [190]Bradford Royal infirmary, Bradford, UK. [191]Department of Paediatric Gastroenterology, Hepatology and Nutrition, Royal Hospital for Children, Glasgow, UK. [192]Avon and Wiltshire Mental Health Partnership NHS Trust, Bath, UK. [193]Queen Elizabeth University Hospital, Glasgow, UK. [194]University Hospital Crosshouse, Kilmarnock, UK. [195]Royal Free Hospital, London, UK. [196]Diana Princess of Wales Hospital, Grimsby, UK. [197]King's College Hospital, London, UK. [198]Western General Hospital, Edinburgh, UK. [199]Barnsley Hospital, Barnsley, UK. [200]Bradford Teaching Hospitals NHS Foundation Trust, Bradford, UK. [201]Wye Valley NHS Trust, Hereford, UK. [202]Newcastle upon Tyne Hospitals NHS Foundation Trust, Newcastle upon Tyne, UK. [203]West Cumberland Hospital, Whitehaven, UK. [204]University Hospital of North Durham, Durham, UK. [205]Worthing Hospital, Worthing, UK.

Methods

ISARIC CCP-UK recruitment, Biorepository and DIAMONDS studies

Ethics approval for the ISARIC CCP-UK study was given by the South Central–Oxford C Research Ethics Committee in England (13/SC/0149), the Scotland A Research Ethics Committee (20/SS/0028) and the WHO Ethics Review Committee (RPC571 and RPC572). Thirty-two children aged <16 years were prospectively recruited by written informed consent (parent or guardian) from the ISARIC WHO CCP-UK cohort admitted to hospital with increased transaminase levels (defined as alanine transaminase levels of >400 IU per litre and/or aspartate aminotransferase levels of >400 IU per litre) that was not due to viral hepatitis A–E, AIH or poisoning. Nine patients had available clinical samples for further investigation. Three additional patients had HLA typing performed, but samples were not available for further analysis. Samples for the control groups were obtained from children (aged <16 years) recruited to the DIAMONDS study, an ongoing multi-country study that aims to develop a molecular diagnostic test for the rapid diagnosis of severe infection and inflammatory diseases using personalized gene signatures (ISRCTN12394803). Ethics approval was given by the London-Dulwich Research Ethics Committee (20/HRA/1714). Controls included healthy individuals (n = 13; group 1), children with PCR-confirmed adenoviral infection with normal transaminase levels (n = 12; group 2), and children with increased transaminase levels without adenoviral infection (n = 33; group 3), recruited between 19 May 2020 to 8 January 2022. Surplus plasma samples from individuals in Scotland (aged <10 years; March to April 2022; group 4) and liver biopsy control samples (from individuals aged <18 years; January 2021 to July 2022) from the Diagnostic Pathology/Blood Sciences archive were obtained with NHS GG&C Biorepository approval (application no. 717; REC 22/WS/0020). Samples from adults that had tested negative by PCR for SARS-CoV-2 were used as an additional group for serological analysis of coronaviruses as a negative control group, also with NHS GG&C Biorepository approval. These adult samples were used without consent on the basis of Human Tissue Act legislation on consent exemption.

Viral PCR

RNA extraction was carried out using the protocol from Biomerieux Easymag. In total, 300 µl of plasma or sera was extracted and eluted into 80 µl of water.

AAV2 RT–qPCR was performed to detect a 62 bp amplicon of the AAV2 inverted terminal repeat region (ITR) as previously described[31] using the forward ITR primer (5′-GGAACCCCTAGTGATGGAGTT-3′) and the reverse ITR primer (5′-CGGCCTCAGTGAGCGA-3′). The AAV2 ITR hydrolysis probe was labelled with fluorescein (6FAM) and quenched with Black Hole quencher (BHQ) 5′-[6FAM]-CA CTCCCTCTCTGCGCGCTCG-[BHQ1]3′). AAV2 primers and probe were synthesized by Merck Life Sciences. RT–qPCR analysis was performed using an ABI7500 Fast Real-Time PCR system (Applied Biosystems). A LUNA Universal One-Step RT PCR kit (New England Biolabs) was used for the amplification and detection of the AAV2 ITR target. RT–qPCR assays were performed in a 20 µl volume reaction (Luna Universal One-Step reaction mix, Luna WarmStart RT enzyme mix, 400 nM forward and reverse primers, 200 nM AAV2 ITR probe and 1–2.5 µl of template DNA) as per the manufacturer's instructions. To quantify the number of copies, serial dilutions of plasmid containing the 62 bp ITR product were used to generate a standard curve, which was then used to interpolate the copy number of AAV2 copies in the samples. Wells with no template were used as negative controls. RT–qPCR reactions were performed in triplicate. The RT–qPCR program consisted of an initial reverse transcription step at 55 °C for 10 min, an initial denaturation step at 95 °C for 1 min followed by 45 cycles of 95 °C denaturation for 10 s and extension at 58 °C for 1 min. A qPCR detection limit between 31 and 32 cycles was calculated as the threshold Ct value at the last dilution of DNA standards that were within the linear range. A PCR result was considered positive if all three reactions tested positive at ≤31 cycles.

Digital droplet PCR was performed according to the manufacturer's instructions using the digital droplet PCR supermix for probes (no dUTP) (Bio-Rad, 1863023) and analysed using a QX200 Droplet Digital PCR system (Bio-Rad, 1864001).

The West of Scotland Specialist Virology Centre, NHS Greater Glasgow and Clyde, conducted diagnostic real-time RT–PCR to detect HAdV, SARS-CoV-2-positive samples and other viral pathogens associated with hepatitis (for example, hepatitis A–E) following nucleic acid extraction utilizing the NucliSENS easyMAG and Roche MG96 platforms. HHV6 (ref. 32) and HAdV41 (ref. 33) were tested by qPCR as previously described using Invitrogen platinum qPCR mix (11730-025) and Quanta Biosciences qPCR mix mastermix (733-1273), respectively, on an ABI7500 system and amplified for 40 cycles. A 6 µl extract was amplified in a total reaction volume of 15 µl.

Measurement of antibody response to coronaviruses by electrochemiluminescence

IgG antibody titres were quantitatively measured against the spike protein, the NTD, the RBD or nucleocapsid of SARS-CoV-2, and against the spike glycoproteins of human seasonal coronaviruses 229E, OC43, NL63 and HKU1 using MSD V-PLEX COVID-19 Coronavirus Panel 2 (K15369) and Respiratory Panel 1 (K15365) kits. Multiplex meso scale discovery electrochemiluminescence (MSD-ECL) assays were performed according to manufacturer's instructions. Samples were diluted 1:5,000 in diluent and added to the plates along with serially diluted reference standard (calibrator) and serology controls 1.1, 1.2 and 1.3. Plates were read using a MESO Sector S 600 plate reader. Data were generated using Methodological Mind software and analysed using MSD Discovery Workbench (v.4.0). Results are expressed as MSD arbitrary units per ml (AU ml^{-1}). Adult negative and positive pools gave the following values: negative pool: spike, 56.6 AU ml^{-1}; NTD, 119.4 AU ml^{-1}; RBD, 110.5 AU ml^{-1}; and nucleocapsid, 20.7 AU ml^{-1}; SARS-CoV-2-positive pool: spike, 1,331.1 AU ml^{-1}; NTD, 1,545.2 AU ml^{-1}; RBD, 1,156.4 AU ml^{-1}; and nucleocapsid, 1,549.0 AU ml^{-1}. In the same assay, NIBSC 20/130 reference serum was used and the following values obtained: spike, 547.7 AU ml$^{-1;}$ NTD, 538.8 AU ml^{-1}; RBD, 536.9 AU ml^{-1}; and nucleocapsid 1,840.2 AU ml^{-1}.

Metagenomics sequencing

Full protocols on the detection of RNA and DNA viruses using metagenomics NGS and TE sequencing methods can be found in refs. 32,34.

In summary, residual nucleic acid from 27 samples from cases with hepatitis (from 9 patients with a combination of plasma, liver, faeces, rectal, and throat and nose samples), 12 samples from HAdV-positive individuals and 13 samples from healthy individuals (control samples were either plasma or sera) underwent metagenomics NGS sequencing at the MRC-University of Glasgow Centre for Virus Research Genomics facility. In brief, each nucleic acid sample was split into two library preparations to improve the chances of detecting RNA and DNA viruses. The protocol used to improve detection of RNA viruses included treatment with DNaseI (Ambion DNase I, ThermoFisher), ribosomal depletion (Ribo-Zero Plus rRNA Depletion Kit, Illumina), except for plasma samples, reverse transcription (SuperScript III, Invitrogen) and double-strand DNA synthesis (NEBNext Ultra II Non-Directional RNA Second Strand Synthesis Module, NEB). The protocol used to detect DNA viruses included partial removal of host DNA (NEBNext Microbiome DNA Enrichment Kit, NEB). Following this, both sets of samples were used to prepare libraries using a KAPA LTP kit (Roche) with unique dual indices (NEBNext Multiplex oligos for Illumina, NEB). The resulting libraries were pooled in equimolar amounts and sequenced using a NextSeq500 (Illumina) to obtain paired-end reads using 150 × 150 cycles.

TE sequencing

Following the library preparation step described above, DNA-derived and RNA-derived libraries were pooled separately and were incubated with VirCapSeq-VERT Capture Panel probes (Roche) following the manufacturer's guidelines. The Roche VirCapSeq-VERT Capture Panel covers the genomes of 207 taxa of viruses known to infect vertebrates (including humans). Enriched DNA-derived and RNA-derived libraries were further amplified using 14 PCR cycles, then pooled and sequenced using a NextSeq500 (Illumina) to obtain paired-end reads using 150 × 150 cycles.

Bioinformatics analysis

Reads for each sample were first quality checked. Illumina adapters were trimmed using Trim Galore (https://github.com/FelixKrueger/TrimGalore) and then mapped to the human genome using BWA-MEM (https://github.com/lh3/bwa). Only reads that did not map to the human genome were used for metagenomics analyses. Reads per million were calculated as the number of viral reads per million reads sequenced to normalize for variation in sample sequencing depth. Non-human reads were then de novo assembled using MetaSPAdes (https://github.com/ablab/spades) to generate contigs for each sample. Contigs were compared against a protein database of all NCBI RefSeq organisms (including virus, bacteria and eukaryotes) with BLASTX using DIAMOND (https://github.com/bbuchfink/diamond). In addition, non-human reads for each sample were aligned to a small panel of HAdV NCBI RefSeq genomes (HAdV-A, HAdV-B1, HAdV-B2, HAdV-C, HAdV-D, HAdV-E, HAdV-F, HAdV-1, HAdV-2, HAdV-5, HAdV-7, HAdV-35, HAdV-54 and HAdV-F41).

The nine AAV2 near-complete genome contigs from the plasma samples were assembled and compared with sequences in GenBank using BLASTN (nucleotide database). Each of these AAV2 genomes had numerous close hits (exhibiting >95% similarity across 95% of the genome) with various existing AAV2 sequences; those most closely related were reported in a previous publication[35]. All linear complete AAV2 genomes returned from BLAST against the GenBank nucleotide database with a query coverage of >75% were selected and combined with the AAV sequences de novo assembled here and aligned using MAFFT. The terminal ends of this alignment were trimmed off, and IQ-TREE 2 was used (TIM+F+R3 model) to infer a phylogenetic tree. For the single HAdV41 genome de novo assembled, all available HAdV41 complete genomes were downloaded from GenBank, aligned with MAFFT and IQ-TREE2 was used (K2P+R2 model) to infer a phylogenetic tree.

Anti-AAV2 ELISA

AAV2 pAAV-CAG-tdTomato viral preparation (codon diversified) was a gift from E. Boyden (Addgene viral preparation number 59462-AAV2; http://n2t.net/addgene:59462; RRID:Addgene_59462).

AAV2 particles, obtained from Addgene (59462-AAV2) were diluted in PBS and used to coat a Immulon 2HB 96-well flat bottom plate (ImmunoChemistry Technologies) at a concentration of 1×10^8 particles per well. The plates were incubated on an orbital shaker overnight at 4 °C. Plates were then blocked with PBS-T (PBS with 0.1% Tween-20) containing 5% BSA for 1 h before the addition of samples. The plates were washed five times in PBS-T before serum samples, diluted 1:50 in PBS, were added in triplicate. A mouse anti-AAV2 (A20, Progen) was used as a positive control at a concentration of 1:50. Samples were incubated at room temperature on an orbital shaker for 90 min before washing five times in PBS-T and adding either anti-human IgM or anti-human IgG (Merck, A9794 and A1543, respectively) diluted 1:10,000. Goat anti-mouse IgG (Merck, A2429) was used as the secondary for the anti-AAV2 A20 positive control. The plates were incubated for 1 h before washing five times with PBS-T then 100 µl of alkaline phosphatase yellow (Merck, P7998) was added and incubated for 15 min before stopping the reaction with 3 M NaOH and the absorbance measured at 405 nm.

Immunohistochemistry, ISH and special staining

Formalin-fixed and paraffin-wax-embedded liver samples were cut at around 3 µm thickness and mounted on glass slides. A reticulin (1936) and Masson trichrome (1929) special staining method (Gordon and Sweets method (1936)) was performed. Antibodies used for immunohistochemistry are listed in Supplementary Table 6.

Detection of viral nucleic acids, ubiquitin and DapB-specific RNA (Advanced Cell Diagnostics, AAV2 (1195791), HHV6 (144565), adenovirus 41 (1192351), ubiquitin (310041) and DapB (310043)) was performed following the manufacturer's protocol with pretreatment with simmering in target solution (30 min) and additional proteinase K (30 min) treatment. A haematoxylin counterstain was performed, and slides were mounted with Vectamount mounting medium (H-500, Vector Laboratories) and scanned using a bright-field slide scanner (Leica, Aperio Versa 8).

Liver histopathology grading

Liver scoring was performed as previously described[8,9].

Quantification of immune cells

After scanning of the whole slide, liver tissue was outlined and the number of positively stained cells (DAB signal for immunohistochemistry or Fast Red signal for ISH) was assessed using software-assisted image analysis (QuPath, v.0.3.2)[36]. For each marker, the cell detection algorithm was tuned, and data were plotted using GraphPad Prism (v.9.4.1).

Spatial analysis (CODEX Phenocycler)

Formalin fixed, paraffin-wax-embedded liver samples (patient 228742A and patient 145808) were sectioned at 2–4 µm thickness on 22 × 22 mm glass coverslips (Akoya Biosciences, 7000005) coated in 0.1% poly-L-lysine (Sigma-Aldrich, P8920). Antigen retrieval was performed by pressure cooking with citrate buffer at pH 6. Carrier-free, pre-conjugated antibodies were purchased directly from Akoya Biosciences or purchased from other suppliers in preparation for custom conjugation. If carrier-free antibodies were not available, alternatives were purchased and purified using a Pierce antibody cleanup kit (44600, ThermoFisher). Antibodies were custom conjugated to a unique oligonucleotide barcode according to the manufacturer's instructions using an antibody conjugation kit (7000009, Akoya Biosciences) and stored at 4 °C for at least 48 h before use. Conjugated antibodies were stored at 4 °C.

Coverslips with tissue were rehydrated in an alcohol series and washed in distilled water before performing heat-induced antigen retrieval in a pressure cooker with citrate buffer (pH 6). Glass coverslips were then moved progressively between wells of a 6-well plate containing components of the CODEX staining kit (Akoya Biosciences, 7000008). This included 2 wells of hydration buffer (2 min each), 1 well of staining buffer (20 min), and then staining with 190 µl of an 11-marker antibody panel (Supplementary Table 7). Tissue sections of both samples were treated in the same way on the same day and were incubated with antibodies for 3 h at room temperature simultaneously. Following staining, tissue was incubated twice in staining buffer (2 min each) and transferred to a post-staining fixation solution made from a 1:10 ratio of paraformaldehyde to storage buffer for 10 min. Tissue samples were then washed 3 times in 1× PBS (14190-094, Gibco), incubated in ice-cold methanol (M/4000/PC17, Fisher Scientific) for 5 min on ice, and again washed 3 times in PBS. Tissue sections were fixed in a fixative solution for 20 min, washed 3× in PBS and stored in storage buffer until image acquisition.

Image acquisition was achieved using a Keyence BZ-X710 microscope equipped with 4 fluorescent channels (1 nuclear stain, 3 for antibody visualization). In a 96-well plate (Akoya Biosciences, 7000006), a maximum of three oligonucleotide reporters were used per well (cycle) (5 µl each) and added to between 235 µl and 245 µl reporter

stock solution that was made according to the manufacturer's instructions. Plates were sealed with aluminium film (Akoya Biosciences, 7000007) and stored at 4 °C until use. Pictures were captured using QuPath (v.0.3.2)[36].

Host genetics and HLA typing

High-resolution typing for all HLA loci (*HLA-A*, *HLA-B*, *HLA-C*, *HLA-DRB1*, *HLA-DRB3*, *HLA-DRB4*, *HLA-DRB5*, *HLA-DQA1*, *HLA-DQB1*, *HLA-DPA1* and *HLA-DPB1*) was performed using an AllType FASTplex NGS assay (One Lambda) run on an Illumina Mi-Seq platform. HLA typing was undertaken on 27 ISARIC participants who provided consent. One patient was omitted from analysis as they were a sibling of another case. HLA types from 64 Scottish National Blood Transfusion Service apheresis platelet donors, self-identified as white British ($n = 15$) or white Scottish ($n = 49$) were used as control samples for comparison with patient HLA allele frequencies. Genotyping was performed using Illumina Global Screening Array v.3.0 + multi-disease beadchips (GSAMD-24v3-0-EA) and Infinium chemistry. This consists of three steps: (1) whole genome amplification; (2) fragmentation followed by hybridization; and (3) single-base extension and staining. Arrays were imaged on an Illumina iScan platform, and genotypes were automatically called using GenomeStudio Analysis software (v.2.0.3), GSAMD-24v3-0-EA_20034606_A1.bpm manifest and a cluster file provided by the manufacturer.

Given the small sample size, it was not possible to implement quality control processes using GenomeStudio and the manufacturer's published recommendations. As genotyping was conducted using the same genotyping array used for the GenOMICC study, variants that passed quality control for the GenOMICC study were retained as previously described[37]. After further excluding variants with call rates of <95%, a total of 478,692 variants were used for downstream analysis.

Kinship and population structure

To identify close relatives up to third degree, King 2.1 was used, which confirmed the presence of a pair of siblings with no further close relatives identified. Genotypes of 19 patients were combined with imputed genotypes of a subset of unrelated participants from the UK Biobank, which was obtained by removing one individual in each pair with estimated kinship larger than 0.0442. The resulting genotypes were filtered to exclude variants with a mean allele frequency of <5%, a genotype missingness rate of <1.5% and Hardy–Weinberg equilibrium of $P < 10^{-50}$. Principal component analysis was conducted with gcta 1.955 in the set of unrelated individuals with pruned single nucleotide polymorphisms using a window of 1,000 markers, a step size of 50 markers and a r^2 threshold of 0.01. Analyses were performed once including all UK Biobank participants and once including only UK Biobank participants who were born in Scotland (UK Biobank data-field 1647) and of Caucasian genetic ancestry (UK Biobank data-field 22006).

Statistics

Differences between cases and control groups were tested using Fisher's exact test for categorical variables and Mann–Whitney (two tailed) for continuous variables using R studio (v.1.2.5033), R (v.4.1.2) and GraphPad (v.9.0.0).

For coronavirus serology experiments, comparisons were carried out using one-way analysis of variance (ANOVA) and Tukey's multiple comparison test, carried out in GraphPad (v.8.4.3).

HLA analysis used the Bridging ImmunoGenomic Data-Analysis Workflow Gaps (BIGDAWG) R package to derive OR and corrected *P* values for individual HLA alleles[38]. The Bonferroni-corrected *P* value significance threshold, adjusted for multiple comparisons (168 HLA alleles), was $P < 3.0 \times 10^{-4}$.

Figures

Figures were prepared using Microsoft Office Excel 2010, Microsoft Office PowerPoint 2010 and Adobe Illustrator 2022.

Reporting summary

Further information on research design is available in the Nature Portfolio Reporting Summary linked to this article.

Data availability

Datasets generated in the current study are appended as supplementary tables. Data, protocols and all documentation regarding this analysis may be made available to academic researchers after authorization from the independent data access and sharing committee. Clinical data and analysis scripts are available on request to the Independent Data Management and Access Committee at https://isaric4c.net/sample_access. Restrictions apply to the availability of identifiable clinical data. Owing to the relatively small number of cases, de-aggregation of data is potentially disclosive, as is the patient-level line list data. Therefore, a formal data-sharing agreement is required for data access. The Independent Data and Material Access Committee considers requests as they arrive; most responses are made within 28 days. Use of clinical samples are also restricted under ethical approvals obtained for their use. Genome sequences are available at GenBank with accession numbers OP019741–OP019749 for AAV2 and OP019750 for HAdV-F41. Source data are provided with this paper.

Code availability

Freely available bioinformatics and statistical software were used, see links in the Methods section.

31. Aurnhammer, C. et al. Universal real-time PCR for the detection and quantification of adeno-associated virus serotype 2-derived inverted terminal repeat sequences. *Hum. Gene Ther. Methods* **23**, 18–28 (2012).
32. Tong, L. et al. Discovery of RNA and DNA viruses using next-generation sequencing: metagenomics. *protocols.io* https://doi.org/10.17504/protocols.io.261ge34zol47/v1 (2023).
33. van Maarseveen, N. M., Wessels, E., de Brouwer, C. S., Vossen, A. C. & Claas, E. C. Diagnosis of viral gastroenteritis by simultaneous detection of Adenovirus group F, Astrovirus, Rotavirus group A, Norovirus genogroups I and II, and Sapovirus in two internally controlled multiplex real-time PCR assays. *J. Clin. Virol.* **49**, 205–210 (2010).
34. Tong, L. et al. Discovery of RNA and DNA viruses using next-generation sequencing: targeted enrichment. *protocols.io* https://doi.org/10.17504/protocols.io.36wgqj3q3vk5/v1 (2023).
35. La Bella, T. et al. Adeno-associated virus in the liver: natural history and consequences in tumour development. *Gut* **69**, 737–747 (2020).
36. Bankhead, P. et al. QuPath: open source software for digital pathology image analysis. *Sci. Rep.* **7**, 16878 (2017).
37. Pairo-Castineira, E. et al. Genetic mechanisms of critical illness in COVID-19. *Nature* **591**, 92–98 (2021).
38. Pappas, D. J., Marin, W., Hollenbach, J. A. & Mack, S. J. Bridging ImmunoGenomic Data Analysis Workflow Gaps (BIGDAWG): an integrated case–control analysis pipeline. *Hum. Immunol.* **77**, 283–287 (2016).
39. Gautheret-Dejean, A. et al. Development of a real-time polymerase chain reaction assay for the diagnosis of human herpesvirus-6 infection and application to bone marrow transplant patients. *J. Virol. Methods* **100**, 27–35 (2002).

Acknowledgements We wish to acknowledge the contribution of the participating children and their parents who agreed to participate in the ISARIC CCP-UK and DIAMONDS studies, and the research teams who recruited the patients; S. Bennett-Slater from NHS Greater Glasgow and Clyde for assisting with sample location and testing; the histopathology team, Veterinary Diagnostic, University of Glasgow, for excellent technical assistance; P. Murcia for providing resources and advice; P. Olmo for administrative assistance; and E. J. Kremer from the Institut de Génétique Moléculaire de Montpellier, Université de Montpellier and A. Baker, University of Edinburgh, for advice. The work was funded by Public Health Scotland, the National Institute for Health Research (NIHR; award CO-CIN-01) and the Medical Research Council (MRC; grants MR/X010252/1, MC_UU_1201412, MC_UU_12018/12, MC_PC_19059, MC_PC_19025 and MC_PC_22004). DIAMONDS is funded by the European Union Horizon 2020 programme; grant 848196). M.P. acknowledges funding support from the Wellcome Trust (206369/Z/17/Z). M.G.S. acknowledges funding support from The Pandemic Institute, Liverpool and the NIHR Health Protection Research Unit (HPRU) in Emerging and Zoonotic Infections at University of Liverpool, and UK Health Security Agency. J.K.B. acknowledges funding support from a Wellcome Trust Senior Research Fellowship (223164/Z/21/Z), and MC_PC_20029, Sepsis Research (Fiona Elizabeth Agnew Trust), a BBSRC Institute Strategic Programme Grant to the Roslin Institute (BB/P013732/1, BB/P013759/1), and the Intensive Care Society of the United Kingdom. We acknowledge the support of Baillie Gifford and the Baillie Gifford Science Pandemic Hub at the University of Edinburgh. Parts of this research has been conducted using the UK Biobank Resource under project 788 and we would like to acknowledge the assistance

of A. Tenesa in making this possible. Additional replication was also conducted using the UK Biobank Resource (Project 26041). This research was also funded by the National Institute for Health and Care Research (CO-CIN-01) and jointly by NIHR and UK Research and Innovation (CV220-169, MC_PC_19059). The views expressed in this article are those of the author(s) and not necessarily those of UKRI, the NIHR, or the Department of Health and Social Care. We also acknowledge the support of NHS Research Scotland (NRS) Greater Glasgow and Clyde Biorepository team. For the purpose of open access, the author has applied a CC BY public copyright licence to any Author Accepted Manuscript version arising from this submission.

Author contributions A.H., A.d.S.F., J.K.B. and E.C.T. conceived the study. A.H., R.O., D.L.R., P.A., V.H., C.D., B.J.W., D.T., R.B., N.A., J.K.B., J.H., P.H., S.R., C.W. and E.C.T. did the formal analysis. A.H., R.T., P.A., V.H., C.D., L.T., K.S., M.M., J.A., B.J.W., K.R., L.P., L.G., C.E., J.M., K.R., K.M., T.D., M.T.G.H., M.L., M.S.H., D.Y., S.C., M. O'Leary, M.P., D.H., A.M., N.M., A.d.S.F., J.B., D.T., R.B., P.H., M.O., P.C., W.O., M.C. and E.C.T. did the investigation. S.E.M., E.V., T.D., S.J.S., C.J., R.G., A.M., N.M., A.B.-S, M.T.G.H, D.E.-R., M.G.S. and M.L. provided resources. N.A., E.P.-C. and V.V. performed validation. A.H. and E.C.T. wrote the original draft of the manuscript. A.H., R.O., R.T., P.A., L.P., J.M., K.R., K.M., T.D., M.T.G.H., M.L., P.H., M.C., M.L., M.P., D.L.R., A.d.S.F., B.J.W., J.B., M.G.S., D.T., J.K.B. and E.C.T. reviewed and edited the manuscript. R.O., P.A., V.H., C.D., K.R., B.J.W. and E.C.T. visualized the data.

Competing interests The authors declare no competing interests.

Additional information

Supplementary information The online version contains supplementary material available at https://doi.org/10.1038/s41586-023-05948-2.

Correspondence and requests for materials should be addressed to Emma C. Thomson.

Peer review information *Nature* thanks Frank Tacke, Leif Sander and the other, anonymous, reviewer(s) for their contribution to the peer review of this work. Peer reviewer reports are available.

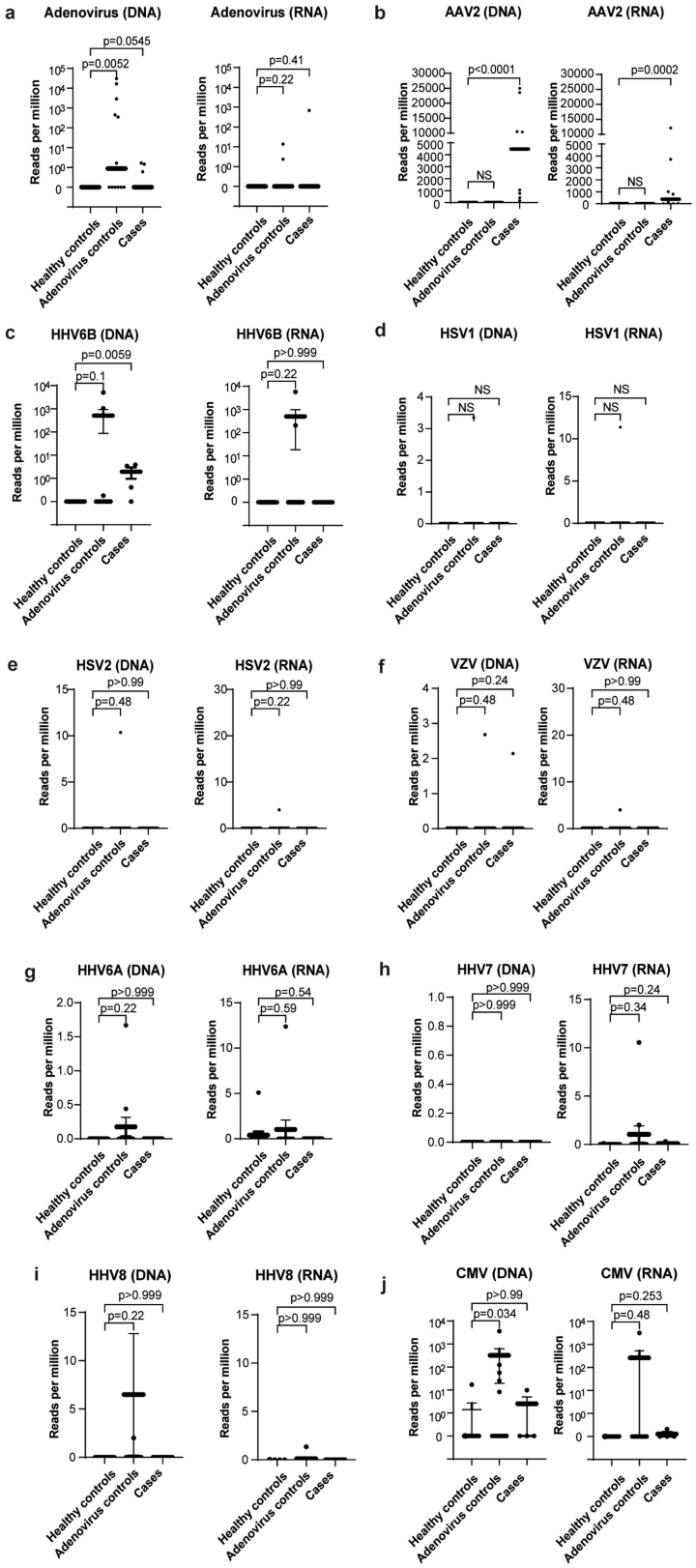

Extended Data Fig. 1 | AAV2, HAdV and human herpesvirus detection by target enrichment sequencing in cases and controls. Read counts per million are plotted for a) HAdV; b) AAV2; c) HHV6B; d) HSV1; e) HSV2; f) VZV; g) HHV6A; h) HHV7; i) HHV8; and j) CMV in cases, Group 1 healthy controls and Group 2 controls (HAdV positive children with normal liver function). Statistical significance was estimated using a Mann-Whitney test (two-sided).

Mutation	Protein	% Cases	% Published
V151A	VP1-3	89	50
Q164N	VP1-3	67	35
R447K	VP1-3	56	6
T450A	VP1-3	56	6
Q457M	VP1-3	100	12
S492A	VP1-3	100	62
E499D	VP1-3	100	15
P521T	VP1-3	89	6
F533Y	VP1-3	100	12
R585S	VP1-3	100	91
R588T	VP1-3	100	94

Mutation	Protein	% Cases	% Published
Q6P	AAP	100	91
E70A	AAP	89	50
P73L	AAP	89	74
T80I	AAP	100	74
S81C	AAP	100	59
N83S	AAP	89	88
K84R	AAP	67	76
I95T	AAP	100	91
L103P	AAP	56	56
F116S	AAP	67	24
H117P	AAP	67	12
D132G	AAP	67	44

Mutation	Protein	% Cases	% Published
T183A	Rep 78, 52	100	94
V508A	Rep 78, 52	100	82
L609V	Rep 78, 52	89	12
F619S	Rep 78, 52	100	94

Extended Data Fig. 2 | Phylogenetic and sequence analysis of AAV2 genomes. a) Maximum likelihood phylogeny of AAV2 from hepatitis cases CVR1-9. The nine AAV2 genome sequences generated from the plasma samples via target enrichment (highlighted in green) were aligned with a range of the closest AAV GenBank sequences[39]. AAV2 reference sequences are denoted by accession number, country and year of sampling b), Phylogeny of HAdV41 genome from case 5. The HAdV41 genome sequence from the faecal sample of patient 5 (red) was combined with complete genomes of HAdV41 from GenBank. Bootstrap values >70 are indicated. HAdV41 reference sequences are denoted by accession number, country and year of sampling; c), Key mutations and hierarchical clustering of AAV2 genomes. Mutations in published AAV2 sequences are highlighted in (blue) and case sequences (green); d) Mutations over-represented in hepatitis cases versus controls. Mutations in VP1-3, Rep78 and 52 and AAP are highlighted by % representation in case sequences (green) and published sequences (blue).

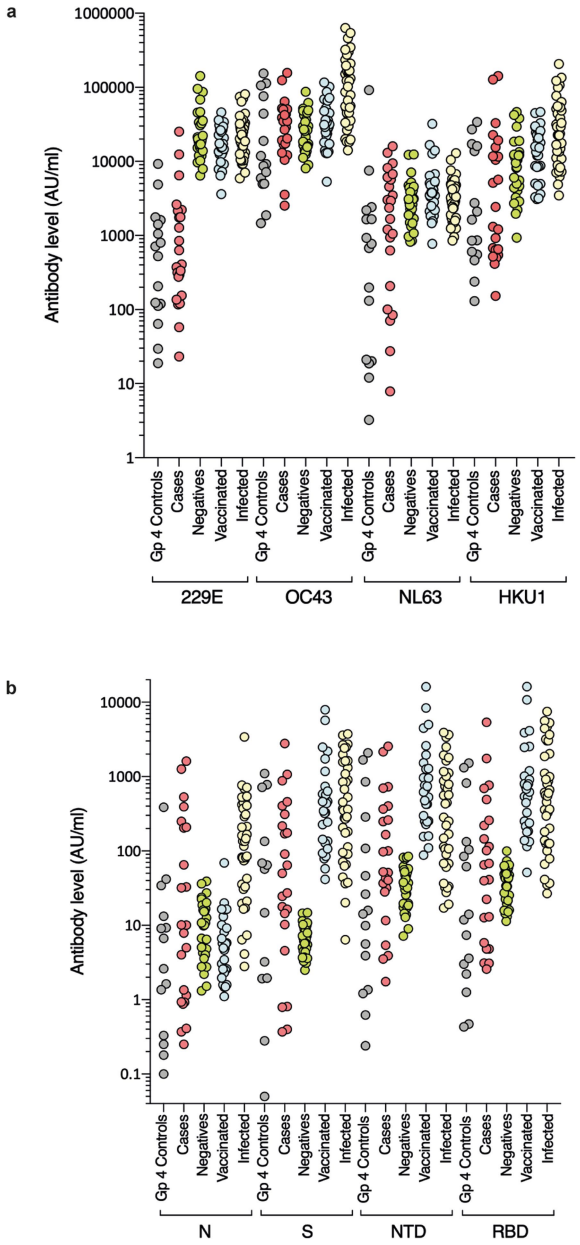

Extended Data Fig. 3 | Reactivity of sera from paediatric hepatitis cases against human seasonal coronaviruses and SARS-CoV-2. Sera from the paediatric hepatitis cases were screened for reactivity against spike proteins from **a)** seasonal coronaviruses 229E, OC43, NL63 and HKU1, and **b**) SARS-CoV-2 nucleocapsid (N), spike (S), and N-terminal domain (NTD) and receptor binding domain (RBD) of S by electrochemiluminescence (MSD-ECL). Reactivity of the 23 samples (Hepatitis) was compared with 16 sera from contemporaneous control samples from children (Group 4 Controls), and three groups of sera from adults of known SARS-CoV-2 status; Negatives (never tested positive for SARS-CoV-2; n = 30), Vaccinated two doses (n = 28) and Infected (n = 39).

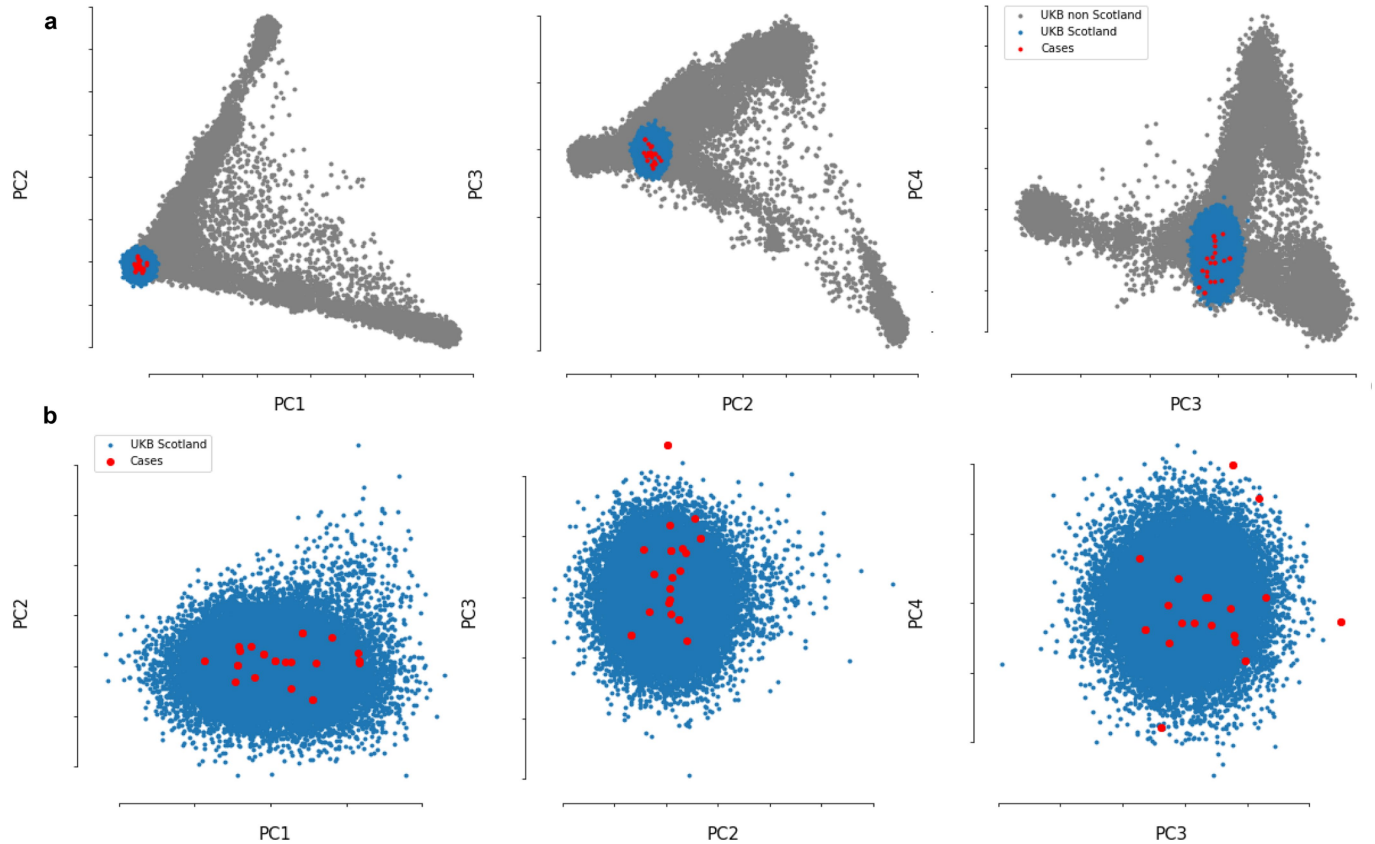

Extended Data Fig. 4 | Principal component analysis (PCA) plots. PCA plots showing the first four genome-wide principal components to confirm genetic ancestry matching. **a)** Genomic PCA using full United Kingdom Biobank cohort as background population (grey), showing the subgroup of unrelated United Kingdom Biobank participants who were born in Scotland and of Caucasian ancestry (blue) and the hepatitis cases reported here (red). **b)** plots showing only the subgroup born in Scotland and of Caucasian ancestry.

Extended Data Table 1 | Modified hepatic activity index scores

	CVR1	CVR3	CVR4	CVR9	CVR35
Modified Ishak score	6/18	10/18	10/18	8/18	11/18
Portal inflammation	2/4	4/4	4/4	2/4	2/4
Interface hepatitis	2/4	4/4	4/4	4/4	4/4
Confluent necrosis	0/6	0/6	0/6	0/6	1/6
Lobular inflammation	2/4	2/4	2/4	2/4	4/4

Extended Data Table 2 | Characteristics of cases and controls a) used in metagenomic and target enrichment analysis b) used in PCR analysis

a

	Cases - metagenomic & TE sequencing analysis (n=9)	**Controls**			
		Group 1 DIAMONDS Healthy (n=13)	P value*	Group 2 DIAMONDS HAdV infection with normal transaminases (N=12)	P value*
Sex - male	4 (44.4)	10 (76.9)	0.19	7 (58.3)	0.67
Age (years)	3.9 (3.4-5.1)	4.1 (3.6-4.8)	0.87	1.4 (1.1-3.1)	0.0006
Recruitment period	14 March – 20 April 2022	6 Nov 2020 - 6 Jul 2021	-	22 May 2020 - 22 Dec 2021	-

b

	Cases – PCR (n=32)	**Controls**							
		Group 1 DIAMONDS Healthy (n=13)	P value*	Group 2 DIAMONDS HAdV infection with normal transaminases (N=12)	P value*	Group 3 DIAMONDS Elevated transaminases with no HAdV infection (n=33)	P value*	Group 4 Scottish hospitalised controls (n=16)	P value*
Sex - male	11 (34.4)	10 (76.9)	0.019	7 (58.3)	0.18	17 (51.5)	0.21	-	-
Age (years) †	4.1 (2.7-5.5)	4.1 (3.6-4.8)	0.95	1.4 (1.1-3.1)	0.0002	10.2 (7-13.6)	<0.0001	-	-
Recruitment period	14 March – 20 August 2022	6 Nov 2020 - 6 Jul 2021	-	22 May 2020 - 22 Dec 2021	-	9 Sep 2020 - 8 Jan 2022	-	12 March - 4 April 2022	-

*Fisher's Exact or chi-squared test for categorical and Mann-Whitney (two-sided) test for continuous variables.

†Age and sex of Group 4 controls unavailable.

nature portfolio

Corresponding author(s): Emma Thomson

Last updated by author(s): Dec 14, 2022

Reporting Summary

Nature Portfolio wishes to improve the reproducibility of the work that we publish. This form provides structure for consistency and transparency in reporting. For further information on Nature Portfolio policies, see our Editorial Policies and the Editorial Policy Checklist.

Statistics

For all statistical analyses, confirm that the following items are present in the figure legend, table legend, main text, or Methods section.

n/a	Confirmed
☐	☒ The exact sample size (*n*) for each experimental group/condition, given as a discrete number and unit of measurement
☐	☒ A statement on whether measurements were taken from distinct samples or whether the same sample was measured repeatedly
☐	☒ The statistical test(s) used AND whether they are one- or two-sided *Only common tests should be described solely by name; describe more complex techniques in the Methods section.*
☒	☐ A description of all covariates tested
☐	☒ A description of any assumptions or corrections, such as tests of normality and adjustment for multiple comparisons
☐	☒ A full description of the statistical parameters including central tendency (e.g. means) or other basic estimates (e.g. regression coefficient) AND variation (e.g. standard deviation) or associated estimates of uncertainty (e.g. confidence intervals)
☐	☒ For null hypothesis testing, the test statistic (e.g. *F*, *t*, *r*) with confidence intervals, effect sizes, degrees of freedom and *P* value noted *Give P values as exact values whenever suitable.*
☒	☐ For Bayesian analysis, information on the choice of priors and Markov chain Monte Carlo settings
☒	☐ For hierarchical and complex designs, identification of the appropriate level for tests and full reporting of outcomes
☒	☐ Estimates of effect sizes (e.g. Cohen's *d*, Pearson's *r*), indicating how they were calculated

Our web collection on statistics for biologists contains articles on many of the points above.

Software and code

Policy information about availability of computer code

Data collection

No commercial code was used for data collection in this study

Data analysis

HLA ANALYSIS
The Bridging ImmunoGenomic Data-Analysis Workflow Gaps (BIGDAWG) R package to derive OR and corrected p values for individual HLA alleles.30 Bonferroni corrected p value significance threshold, adjusted for multiple comparisons (168 HLA alleles), was p < 3.0×10−4.

BIOINFORMATICS ANALYSIS
Reads for each sample were first quality checked, Illumina adapters were trimmed using Trim Galore version 0.6.6 (https://github.com/FelixKrueger/TrimGalore), and reads were then mapped to the human genome using BWA-MEM version 0.7.17 (https://github.com/lh3/bwa). Only reads that did not map to the human genome were used for metagenomic analyses. Non-human reads were then de novo assembled using MetaSPAdes version 3.15.5 (https://github.com/ablab/spades) to generate contigs for each sample. Contigs were then compared against a protein database of all NCBI RefSeq organisms (including virus, bacteria, eukaryotes) with BLASTX using DIAMOND version 2.0.15 (https://github.com/bbuchfink/diamond). In addition, non-human reads for each sample were aligned to a small panel of HAdV NCBI RefSeq genomes (HAdV-A, B1, B2, C, D, E, F, 1, 2, 5, 7, 35, 54 as well as HAdV-F41).

STATISTICAL ANALYSIS
Differences between cases and control groups were tested using Fisher's Exact Test for categorical variables and Mann-Whitney (two tailed) for continuous variables. Spearman's rank correlation coefficients were calculated for the relationships between the trajectories of viral load and ALT and bilirubin. We used R studio version 1.2.5033, R version 4.1.2 and GraphPad version 9.0.0 for most statistical analyses. For coronavirus serology experiments, comparisons were carried out with one way ANOVA and Tukey's Multiple Comparison test, carried out in

GraphPad version 8.4.3.

For manuscripts utilizing custom algorithms or software that are central to the research but not yet described in published literature, software must be made available to editors and reviewers. We strongly encourage code deposition in a community repository (e.g. GitHub). See the Nature Portfolio guidelines for submitting code & software for further information.

Data

Policy information about availability of data

All manuscripts must include a data availability statement. This statement should provide the following information, where applicable:

- Accession codes, unique identifiers, or web links for publicly available datasets
- A description of any restrictions on data availability
- For clinical datasets or third party data, please ensure that the statement adheres to our policy

Datasets generated in the current study are appended as Source Data, Extended Data Tables and Supplementary Tables. Data, protocols, and all documentation around this analysis may be made available to academic researchers after authorisation from the independent data access and sharing committee. Clinical data and analysis scripts are available on request to the Independent Data Management and Access Committee at https://isaric4c.net/ sample_access. Restrictions apply to the availability of identifiable clinical data. Due to the relatively small number of cases, de-aggregation of data is potentially disclosive, as is the patient-level line list data. Therefore, a formal data sharing agreement is required for data access. The Independent Data and Material Access Committee considers requests as they arrive; most responses are made within 28 days. Use of clinical samples are also restricted under ethical approvals obtained for their use. Genome sequences are available in GenBank with accession numbers for AAV2: OP019741-OP019749 and for HAdV-F41: OP019750.

Human research participants

Policy information about studies involving human research participants and Sex and Gender in Research.

Reporting on sex and gender	For the case control study, recruited patients were female (n=20) and male (n=12). Group 1 healthy control subjects were restricted to 13 children recruited in the UK between January 2020 and April 2022 and were age-matched but not sex-matched due to availability of samples (10 male, 3 female; age range 3-5 years). Group 2 subjects were children (8 male, 4 female; age range 1-4 years) with PCR-confirmed HAdV infection and normal transaminases Group 3, 33 children (18 male, 15 female; age range 2-16 years) with raised transaminases who were HAdV PCR negative. Group 4 included 16 residual samples from children from the NHS GG&C biorepository aged <18 years. Further information was not available under ethical protocols for the use of residual biorepository samples. For the HLA analysis a further 3 cases were recruited to the ISARIC CCP-UK cohort and had HLA typing carried out but further clinical samples and additional clinical data were not available.
Population characteristics	The median age of affected patients was 4.1 years (IQR: 2.7 to 5.5 years) (Table 1). Twenty of the 32 (63%) children were female, and all were of white ethnicity. Eighteen (56%) of the children reported a subacute history 2-12 weeks prior to acute hepatitis, characterised by an initial gastroenteritis-like illness followed by intermittent vomiting, abdominal pain and fatigue. Most of the affected children (23/32) had no other medical conditions: one child had previously received a liver transplant; none of the other cases were immunocompromised and none had received COVID-19 vaccination. All routine blood tests for viral hepatitis, including hepatitis A, B, C, E, acute Epstein-Barr virus (EBV), cytomegalovirus (CMV), human herpes virus (HHV) 6/7 and herpes simplex virus (HSV) were negative
Recruitment	To investigate the aetiology of the acute hepatitis cases, we recruited 32 of the earliest affected children who presented to hospital between 14 March and 4 April 2022 into the International Severe Acute Respiratory and Emerging Infections Consortium (ISARIC) WHO Clinical Characterisation Protocol UK (CCP-UK) [ISRCTN 66726260]7. All cases who fulfilled the case definition and were willing to participate were recruited. For the HLA analysis a further 3 cases were recruited to the ISARIC CCP-UK cohort and had HLA typing carried out but further clinical samples and additional clinical data were not available. Control samples (Groups 1,2 and 3) were obtained from the Diagnosis and Management of Febrile Illness using RNA Personalised Molecular Signature Diagnosis study cohort (DIAMONDS; https://www.diamonds2020.eu). This study recruited children presenting with suspected infection or inflammation. Patients were recruited with the informed written consent of parents or guardians.
Ethics oversight	32 affected children, who presented to hospital between 14 March and 20 August 2022 and who met the PHS case definition into the International Severe Acute Respiratory and Emerging Infections Consortium (ISARIC) WHO Clinical Characterisation Protocol UK (CCP-UK) [ISRCTN 66726260].7 Ethical approval was given by the South Central–Oxford C Research Ethics Committee in England (13/SC/0149), the Scotland A Research Ethics Committee (20/SS/0028), and the WHO Ethics Review Committee (RPC571 and RPC572). Control samples (Groups 1-3) were obtained from the Diagnosis and Management of Febrile Illness using RNA Personalised Molecular Signature Diagnosis study cohort (DIAMONDS; https://www.diamonds2020.eu). Patients were recruited with the written informed consent of parents or guardians. Contemporaneous Scottish surplus plasma and liver biopsy control samples (Control Group 4) from the Diagnostic Pathology/ Blood Sciences archive were obtained with NHS GG&C Biorepository approval (application #717; REC 22/WS/0020). These samples were used without consent following HTA legislation on consent exemption. Genetic (HLA) control data was obtained using the UK Biobank Resource (project 788; 21/NW/0157). Participants in the UK Biobank have been recruited with written informed consent.

Note that full information on the approval of the study protocol must also be provided in the manuscript.

Field-specific reporting

Please select the one below that is the best fit for your research. If you are not sure, read the appropriate sections before making your selection.

☒ Life sciences ☐ Behavioural & social sciences ☐ Ecological, evolutionary & environmental sciences

For a reference copy of the document with all sections, see nature.com/documents/nr-reporting-summary-flat.pdf

Life sciences study design

All studies must disclose on these points even when the disclosure is negative.

Sample size	All available cases were selected. All available healthy control samples that could be age-matched to cases were obtained from the DIAMONDS cohort (we planned for up to a 1-3:1 ratio of controls:cases). We selected all available control subjects in group 2 (HAdV positive with normal LFTs) from the DIAMONDS cohort. These were all children but were not age matched. We also selected all available control subject samples in group 3 (hepatitis of alternative aetiology) from the DIAMONDS cohort. We used all available residual samples from children from the same time period as cases in group 4.
Data exclusions	We excluded any cases that did not meet the PHS definition for non-A-E paediatric hepatitis on the basis of age (over 10 years of age or with an alternative diagnosis or from whom clinical data was not available). We excluded 5 plasma samples in the case control study from the NGS analysis of herpesviruses because during nucleic extraction in the relevant clinical laboratory, murine cytomegalovirus (CMV) had been used as an extraction control. This was not used for other sample extractions in the case control study. Clinical specimens taken from cases (throat, rectal swab, faeces and liver samples) also had murine CMV added to the samples and were also excluded from the NGS herpes read count analysis. However, all samples were tested for human herpesviruses by PCR.
Replication	PCR experiments were carried out in triplicate, other than GAPDH PCR which was carried out in duplicate or triplicate. Results were highly concordant. There were four AAV2 Ct values that were borderline (traversing the limit of detection). These were considered negative as weakly positive results were not reproducible and read counts for all samples were negative by metagenomic and target enrichment NGS. Next generation sequencing experiments were repeated on separate runs using different methods (metagenomic sequencing and then semi-agnostic target enrichment sequencing). Results were also confirmed by PCR for AAV2, HAdV and HHV6.
Randomization	As described above, all available cases were selected. All available healthy control samples that could be age-matched to cases were obtained from the DIAMONDS cohort (we planned for up to a 1-3:1 ratio of controls:cases). We selected all available control subjects in group 2 (HAdV positive with normal LFTs) from the DIAMONDS cohort. These were all children but were not age matched. We also selected all available control subject samples in group 3 (hepatitis of alternative aetiology) from the DIAMONDS cohort.
Blinding	The first sequencing run was of samples from 5 cases carried out urgently at the request of Public Health Scotland and investigators were not blinded to these as ethical permissions were not in place for the use of control samples. Subsequent runs were carried out when control samples were available and included 4 further cases. These were analysed with blinding of case/control status and then samples were compared to look for viruses present in cases and controls. PCR, serology and histology experiments were carried out with blinding in place.

Reporting for specific materials, systems and methods

We require information from authors about some types of materials, experimental systems and methods used in many studies. Here, indicate whether each material, system or method listed is relevant to your study. If you are not sure if a list item applies to your research, read the appropriate section before selecting a response.

Materials & experimental systems

n/a	Involved in the study
☐	☒ Antibodies
☒	☐ Eukaryotic cell lines
☒	☐ Palaeontology and archaeology
☒	☐ Animals and other organisms
☒	☐ Clinical data
☒	☐ Dual use research of concern

Methods

n/a	Involved in the study
☒	☐ ChIP-seq
☒	☐ Flow cytometry
☒	☐ MRI-based neuroimaging

Antibodies

Antibodies used	For AAV2 ELISA, bound human antibody was detected with either anti-human IgM or anti-human IgG (Merck, UK cat no. A9794 and A1543, respectively). Antibodies for IHC are listed below. AAntigen Dilution Clone Product code, company Antigen retrieval Detection system

MHCII 1:200 none M0746, Dako/Agilent Pressure cooking; citrate pH6 Envision Dako Agilent
C4d complement 1:100 none Quidel A213 Antihuman C4d ER2 (20) Leica BOND polymer DS9800 and BOND DAB enhancer
CD3 1:100 LN10 Leica NCL-L-CD3-565 ER2 (20) Leica BOND polymer DS9800 and BOND DAB enhancer
CD4 1:200 1F6 Leica NCL-L-CD4-368 ER2 (20) Leica BOND polymer DS9800 and BOND DAB enhancer
CD8 1:50 4B11 Leica NCL-CD8-4B11 ER2 (20) Leica BOND polymer DS9800 and BOND DAB enhancer
CD20 1:200 L26 Novocastra NCL-L-CD20-L26 ER1 (20) Leica BOND polymer DS9800 and BOND DAB enhancer

Target Ref # Supplier Reporter/Barcode Fluorophore Concentration
CD20 4450018 Akoya Biosciences Bx007 AF750 1/200
CD44 4450041 Akoya Biosciences Bx005 Atto 550 1/100
CD3 4450030 Akoya Biosciences Bx045 Cy5 1/200
PanCK 4450020 Akoya Biosciences Bx019 AF750 1/200
CD31 4450017 Akoya Biosciences Bx001 AF750 1/100
Mx1 M143 Custom made- University Medical Centre Freiburg Bx022 AF 750 1/50
CD8 4250012 Akoya Biosciences BX026 Atto 550 1/200
CD68 4350019 Akoya Biosciences Bx015 Cy5 1/200
CD107a 4350001 Akoya Biosciences Rx006 Cy5 1/200
CD4 4350018 Akoya Biosciences Bx003 cy5 1/200

Validation

For IHC, C4d was validated on Kidney with acute rejection versus normal kidney tissue. Validation policies and procedures were carried out in accordance with ISO accreditation ISO 15189. CD3, CD4, CD8 and CD20 were validated with normal tonsil control tissue and positive case tissue (lymphoma) from a minimum of 3 cases. Procedures were carried out in accordance with ISO 15189. Test subject tissue for these cases was compared with normal controls and negative controls.
For the CODEX analysis, we carried out validation of antibodies by 1.) replacing the primary antibody with isotype serum and 2.) checking in each section that stained cells had the morphology of the cell to be stained, e.g. MHCII macrophage-like cells close to the sinus using concentrations, as recommended by the manufacturer.